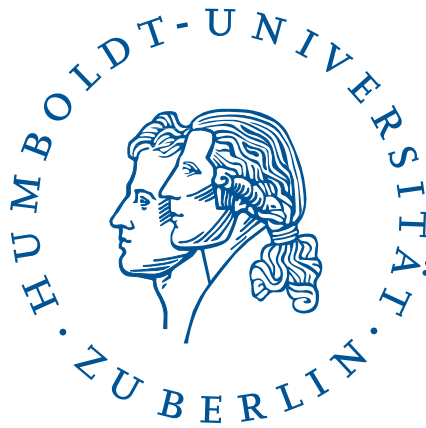# Optical excitations in rutile and anatase TiO$_2$ investigated by many-body perturbation theory

MASTERARBEIT

zur Erlangung des akademischen Grades
Master of Science
(M. Sc.)
im Fach Physik

eingereicht an der
Mathematisch-Naturwissenschaftlichen Fakultät I
Institut für Physik
Humboldt-Universität zu Berlin

von
Frau Olga Turkina
geboren am 28.11.1988 in Charkow, Ukraine

Betreuer: *Prof. Dr. Claudia Ambrosch-Draxl*
Gutachter: *Prof. Dr. Fritz Henneberger*

eingereicht am: *24. Dezember 2013*

Contents

Introduction

First principle investigations are an indispensable tool for understanding the properties of existing materials and application-oriented design of new ones. In the past decades the theoretical research of electronic, optical and chemical properties of materials has made great improvements by combined use of theoretical developments and computer simulations. Deep insight into the properties of complex solid state materials are made possible by the development of theoretical techniques such as the density functional theory (DFT) and the many-body perturbation theory (MBPT). The density functional theory has proven to yield a great number of ground-state properties in an accurate manner. To obtain the excited state properties of systems, one has to go beyond DFT and employ the many-body perturbation theory that uses DFT calculations as a starting point.

In this thesis we want to apply both methodologies to investigate the single-crystal polymorphs of TiO_2 – rutile and anatase – with the goal of describing the optical properties of this semiconductor material. TiO_2 is of interest in the current research – because of its low cost and availability it is used in photocatalysis, as an electron-transporting substrate in dye-sensitized solar cells, and is considered for use as an active material in solar-energy conversion.

By means of this study we also want to investigate the following problem. DFT is by construction an exact ground-state theory. However, as we will see, a central approximation must be made when adapting the DFT to practical calculations. The complicated many-body effects of the system are contained in the so-called exchange-correlation energy functional that is not known exactly and has to be approximated. The quality of this approximation determines the quality of the results of the ground-state calculation. We want to investigate whether a different type of an approximation to this functional play a significant role in the determination of excited-state properties of the system as well. In other words, the starting point dependence of MBPT is analyzed.

The work is organized as follows. In Chapter 1 the main concepts of DFT are outlined. We start by explaining the theorems proven by Hohenberg and Kohn [1] that provide the foundation for DFT, and proceed by outlining the Kohn-Sham approach that allows DFT to be implemented in practice. The exchange-correlation approximations are discussed. After a detailed explanation of the reason that DFT cannot be used to determine excited-state properties of systems, we proceed to Chapter 2. There we give an overview over the many-body perturbation theory. First, the G_0W_0 method is discussed. It is used for calculation of single-particle

excitations allowing us to compute band structures. The Bethe-Salpeter formalism presented next allows for calculation of optical absorption spectra including excitonic effects. Chapter 3 gives a short overview over the all-electron full-potential (L)APW+lo method is given. The method allows to represent the quantities of an electronic structure calculation in a basis set. Chapter 4 is devoted to the discussion of the results. For the calculations we use the **exciting** code [2].

A summary of the findings and an outlook towards possible improvements of the presented theory and development of other methodologies close the thesis.

Chapter 1

Density functional theory

1.1 The many-body problem

The fundamental task of solid-state physics consists of solving the Schrödinger equation for the Hamiltonian describing an interacting system of electrons and nuclei:

$$\hat{\mathscr{H}} = -\sum_i \frac{\hbar^2 \nabla_i^2}{2m_e} - \sum_I \frac{\hbar^2 \nabla_I^2}{2M_I} + \frac{1}{2}\sum_{i \neq j} \frac{e^2}{|\mathbf{r}_i - \mathbf{r}_j|} - \sum_{i,I} \frac{Z_I e^2}{|\mathbf{r}_i - \mathbf{R}_I|} + \frac{1}{2}\sum_{i \neq I} \frac{Z_I Z_J e^2}{|\mathbf{R}_I - \mathbf{R}_J|}, \quad (1.1)$$

where $\mathbf{R}_I$, Z_I and M_I are the coordinates, the atomic number and the mass of the nucleus I, respectively, $\mathbf{r}_i$, e, m_e are the coordinates, the charge and the mass of the electron i. Considering that the number of coupled differential equations contained in this Hamiltonian is of the order of the Avogadro number $\sim 10^{23}$ for a macroscopic solid, diagonalizing it is enormously complex. Inevitably, approximations must be made. The Born-Oppenheimer approximation that is also called *adiabatic* approximation is employed in almost all studies of solids. It utilizes the fact that the motion of the electrons is orders of magnitude faster that of the nuclei due to the vast mass difference between them. It is thus justified to separate the motion of the electrons from that of the nuclei allowing us to consider the problem of interacting electrons in a potential generated by the ions fixed at the positions $\mathbf{R}_I$[1]:

$$\begin{aligned}
\hat{H} &= -\sum_i \frac{\nabla_i^2}{2} - \sum_{i,I} \frac{Z_I}{|\mathbf{r}_i - \mathbf{R}_I|} + \frac{1}{2}\sum_{i \neq j} \frac{1}{|\mathbf{r}_i - \mathbf{r}_j|} \\
&= \hat{T} + \hat{V}_{ext} + \hat{V}_{ee}.
\end{aligned} \quad (1.2)$$

There are various conceptually different approaches to this problem. Among the first ideas was Hartree's proposition to approximate the N-electron wave function $\Psi(\mathbf{r}_1, \mathbf{r}_2, ..., \mathbf{r}_N)$, where $\mathbf{r}_i$ denotes spatial coordinates and the spin coordinate of the i-th electron, by a product of single-particle wave functions $\psi_i(\mathbf{r}_i)$. In this manner the problem is reduced to solving N single-particle Schrödinger equations. This *ansatz* was later extended in the Hartree-Fock theory to include the Fermi statistics in the

---

[1]Henceforth atomic units shall be used: $\hbar = 1, e = 1, m_e = 1, a_0 = 1$.

many-electron wave function represented by the so-called Slater determinant. It can be further improved upon by taking into account excited configurations in a linear combination of Slater determinants which is known as Configuration Interaction. All of these methods aim at computing the wave function directly, as the latter can be used to calculate the expectation values of observables in a straightforward manner. Unfortunately, the computational complexity of these wave-function based approaches grows tremendously with the number of electrons.

However, it is not necessary to know the full many-electron wave function if one is only interested in obtaining observables such as the total energy. The ground-state electron density $\rho(\mathbf{r})$, an "integrated" variable

$$\rho(\mathbf{r}) = N \int d\mathbf{r}_2 ... d\mathbf{r}_N \, |\Psi_0(\mathbf{r}, \mathbf{r}_2, ..., \mathbf{r}_N)|^2, \tag{1.3}$$

where Ψ_0 is the ground-state wave function, is sufficient to describe the ground state of an electronic system. The electron density is the central quantity of density-functional theory (DFT), which is used for computation of the ground-state properties of the systems considered in this thesis.

In the following, we shall outline the basic ideas of DFT, the necessary approximations for practical application of DFT, its achievements and inherent limitations.[2]

1.2   The Hohenberg-Kohn theorems

The idea to use the ground-state density stems from independent works of Thomas and Fermi in the early age of quantum mechanics. Under the assumption of uncorrelated electron motion they approximated the kinetic energy by the noninteracting homogeneous electron gas, which is a function of the density $\varepsilon_{kin} \sim \rho^{\frac{2}{3}}$. Although this approach could not be very successfully applied to real materials, it is regarded as an origin of DFT.

The theoretical justification for using the density as a basic variable was given in 1964 by Hohenberg and Kohn [1]. They proved a fundamental theorem of DFT known as the Hohenberg-Kohn theorem. The theorem states that for a bound interacting system of fermions in a static external potential $\hat{V}_{ext} = \sum_i v_{ext}(\mathbf{r}_i)$ a one-to-one correspondence up to an arbitrary additive constant exists between the ground-state density $\rho(\mathbf{r})$ and the potential V_{ext}.

The proof is by *reductio ad absurdum*, assuming the existence of two potentials $v_{ext,1}(\mathbf{r})$ and $v_{ext,2}(\mathbf{r})$ (differing not by a constant) that lead to the same non-degenerate ground-state density $\rho(\mathbf{r})$. Let $\hat{H}_1$ be the Hamiltonian of the structure

---

[2]We will restrict ourselves to addressing density-functional theory for spin-unpolarized systems as it was originally developed. The term 'spin-unpolarized' refers to systems containing equal number of electrons with spin-up and spin-down polarizations and subjected to a spin-independent external potential, so that no spin effects have to be accounted for. In practice, spin-polarized systems are often encountered, for example systems with an odd number of electrons. In that case spin-polarized DFT is applied, a generalization of DFT that distinguishes between the spin-up and spin-down electron density.

(1.2) corresponding to the external potential $v_{ext,1}(\mathbf{r})$ and its ground state be defined by the many-body wave function Ψ_1 and the energy E_1. The ground state of $\hat{H}_2$ containing $v_{ext,2}(\mathbf{r})$ is defined by Ψ_2 and E_2 accordingly. The ground-state energy of each system can be expressed as the expectation value of the respective Hamiltonian:

$$E_{1,2} = \langle \Psi_{1,2} | \hat{T} + \hat{V}_{ee} | \Psi_{1,2} \rangle + \int d\mathbf{r}\, \rho(\mathbf{r})\, v_{ext,1,2}(\mathbf{r}). \qquad (1.4)$$

Now consider the Raleigh-Ritz minimal principle for the ground state of $\hat{H}_1$:

$$\begin{aligned}
E_1 &< \langle \Psi_2 | \hat{H}_1 | \Psi_2 \rangle \\
&= \langle \Psi_2 | \hat{T} + \hat{V}_{ee} | \Psi_2 \rangle + \int d\mathbf{r}\, \rho(\mathbf{r})\, v_{ext,1}(\mathbf{r}) \\
&= E_2 + \int d\mathbf{r}\, \rho(\mathbf{r}) \left[v_{ext,1}(\mathbf{r}) - v_{ext,2}(\mathbf{r}) \right].
\end{aligned} \qquad (1.5)$$

For the ground state of $\hat{H}_2$ the analogous reasoning applies:

$$E_2 < E_1 + \int d\mathbf{r}\, \rho(\mathbf{r}) \left[v_{ext,2}(\mathbf{r}) - v_{ext,1}(\mathbf{r}) \right]. \qquad (1.6)$$

Adding Eqs. (1.5) and (1.6) we arrive at a contradiction

$$E_1 + E_2 < E_1 + E_2, \qquad (1.7)$$

hence the assumption of the existence of the second potential leading to the same ground-state density is wrong and the theorem hereby proven. The proof for a degenerate ground-state can be found in the original paper [1].

Since the operators for the kinetic term $\hat{T}$ and the Coulomb interaction $\hat{V}_{ee}$ (Eq. (1.2)) are identical for all many-electron systems, the theorem establishes a unique correspondence between the Hamiltonian of the system and the ground-state density. Hence the wave function is a functional of the density up to a phase factor. As a consequence, Hohenberg and Kohn state further that the expectation value of any observable of a many-electron system is a functional of the electron density:

$$\langle \Psi_0 | \hat{O} | \Psi_0 \rangle = O[\rho]. \qquad (1.8)$$

In particular the Hohenberg-Kohn minimum principle applies to the ground-state energy E_0. The total energy $E[\rho]$ can be minimized, yielding its minimum value, the ground-state energy, at the ground-state density:

$$E_0[\rho] \leq E[\tilde{\rho}]. \qquad (1.9)$$

This principle can be formulated using the constrained search method developed by Levy [3] and Lieb. Consider the Rayleigh-Ritz minimal principle for the total energy:

$$E_0 = \min_{\{\tilde{\Psi}\}} \langle \tilde{\Psi} | \hat{H} | \tilde{\Psi} \rangle. \qquad (1.10)$$

Let us denote the set of wave functions resulting in a certain density by $\{\Psi(\rho(\mathbf{r}))\}$. Eq. (1.10) can now be rewritten as a density functional

$$
\begin{aligned}
E[\rho] &= \min_{\{\tilde{\Psi}(\tilde{\rho}(\mathbf{r}))\}} \langle \tilde{\Psi}|\hat{H}|\tilde{\Psi}\rangle \\
&= \min_{\{\tilde{\Psi}(\tilde{\rho}(\mathbf{r}))\}} F[\tilde{\rho}(\mathbf{r})] + \int \mathrm{d}\mathbf{r}\, \tilde{\rho}(\mathbf{r})\, v_{ext}(\mathbf{r}),
\end{aligned}
\tag{1.11}
$$

where we take advantage of the fact that all wave functions producing the same density $\rho(\mathbf{r})$ also correspond to the same $\langle \Psi|\hat{V}_{ext}|\Psi\rangle$ in accordance with the Hohenberg-Kohn theorem. $F[\tilde{\rho}]$ is a universal, i.e. system-independent, density functional comprised of kinetic and Coulomb energy:

$$
F[\tilde{\rho}(\mathbf{r})] = \langle \tilde{\Psi}|\hat{T} + \hat{V}_{ee}|\tilde{\Psi}\rangle .
\tag{1.12}
$$

Now we can perform the minimization with respect to the density:

$$
\begin{aligned}
E_0 &= \min_{\{\tilde{\rho}(\mathbf{r})\}} E[\rho] \\
&= \min_{\{\tilde{\rho}(\mathbf{r})\}} \left\{ F[\tilde{\rho}(\mathbf{r})] + \int \mathrm{d}\mathbf{r}\, \tilde{\rho}(\mathbf{r})\, v_{ext}(\mathbf{r}) \right\},
\end{aligned}
\tag{1.13}
$$

obtaining the ground-state energy in accordance with the Hohenberg-Kohn minimum principle.

At this point we have to point out that the above presentation implicitly uses two assumptions. One assumption is that any density is N-representable, *i.e.*, there exists an antisymmetric N-electron wave function generating the density. It can be indeed shown [4] that all non-negative densities that integrate to N fulfill this condition. The other issue is referred to as the v-representability – the question whether for any density there exists an external potential that reproduces this density. Levy [3] and Lieb showed that not all densities are v-representable. Still, in practice, one can generally find a potential within sufficient accuracy. We will assume v-representability throughout the discussion.

Summarizing, we can say that Hohenberg-Kohn theorems demonstrate the validity of a density-based approach to the many-electron problem, however, they do not provide a practical recipe for determining the electron density. Unfortunately, explicit variation of the total energy as shown in Eq. (1.13) is not feasible, since the exact form of $F[\tilde{\rho}]$ is unknown. Let us look at the work of Kohn and Sham [5] who developed a self-consistent scheme for determining the ground-state density.

1.3 The Kohn-Sham equations

The central idea of Kohn and Sham was to map a system of interacting electrons with the Hamiltonian

$$
\hat{H} = \hat{T} + \hat{V}_{ext} + \hat{V}_{ee}
\tag{1.14}
$$

onto a fictitious system of non-interacting electrons that has the same ground-state density that is subject to a potential containing all the many-body effects:

$$\hat{H}' = \hat{T} + \hat{V}_{KS}. \tag{1.15}$$

Thus only a set of single-particle equations need to be solved instead of dealing with a fully interacting Schrödinger equation. The exact form of these equations can be obtained from the interacting system through the following considerations.[3]

Let us first apply the variational principle to the total-energy functional

$$E[\rho] = F[\rho] + \int d\mathbf{r}\, \rho(\mathbf{r})\, v_{ext}(\mathbf{r}), \tag{1.16}$$

keeping the number of electrons N constant by introducing the Lagrange multiplier ε:

$$
\begin{aligned}
\delta E[\tilde{\rho}(\mathbf{r})] &= \int d\mathbf{r}\, \frac{\delta}{\delta\tilde{\rho}(\mathbf{r})} \left[E[\tilde{\rho}(\mathbf{r})] - \left(\varepsilon \int d\mathbf{r}'\, \tilde{\rho}(\mathbf{r}') - N \right) \right] \delta\tilde{\rho}(\mathbf{r}) \\
&= \int d\mathbf{r} \left[\frac{\delta E[\tilde{\rho}(\mathbf{r})]}{\delta\tilde{\rho}(\mathbf{r})} - \varepsilon \right] \delta\tilde{\rho}(\mathbf{r}) \\
&= \int d\mathbf{r} \left[\frac{\delta F[\tilde{\rho}(\mathbf{r})]}{\delta\tilde{\rho}(\mathbf{r})} + v_{ext}(\mathbf{r}) - \varepsilon \right] \delta\tilde{\rho}(\mathbf{r}) = 0.
\end{aligned}
\tag{1.17}
$$

To handle the unknown functional $F[\rho]$ Kohn and Sham suggested to express it as a sum of the kinetic energy of a non-interacting N electron system $T'[\rho]$, the classical Coulomb interaction energy known as the Hartree energy, and a remainder $E_{xc}[\rho]$ called the exchange-correlation energy:

$$F[\rho] = T'[\rho] + \frac{1}{2} \int d\mathbf{r} \int d\mathbf{r}'\, \frac{\rho(\mathbf{r})\,\rho(\mathbf{r}')}{|\mathbf{r} - \mathbf{r}'|} + E_{xc}[\rho]. \tag{1.18}$$

$E_{xc}[\rho]$ is formally defined by the Eqs. (1.16) and (1.18) as

$$E_{xc}[\rho] = T[\rho] + V_{ee}[\rho] - T'[\rho] - \frac{1}{2} \int d\mathbf{r} \int d\mathbf{r}'\, \frac{\rho(\mathbf{r})\,\rho(\mathbf{r}')}{|\mathbf{r} - \mathbf{r}'|}. \tag{1.19}$$

Using this formulation of $F[\rho]$ Eq. (1.17) can be written as

$$\delta E[\tilde{\rho}(\mathbf{r})] = \int d\mathbf{r} \left[\frac{\delta T'[\tilde{\rho}(\mathbf{r})]}{\delta\tilde{\rho}(\mathbf{r})} + v_{KS}(\mathbf{r}) \bigg|_{\tilde{\rho}(\mathbf{r})=\rho(\mathbf{r})} - \varepsilon \right] \delta\tilde{\rho}(\mathbf{r}) = 0, \tag{1.20}$$

defining the Kohn-Sham potential v_{KS} in the following way:

$$v_{KS}(\mathbf{r}) = v_H(\mathbf{r}) + v_{ext}(\mathbf{r}) + v_{xc}[\rho]. \tag{1.21}$$

---

[3]We assume the v-representability of both the interacting and the non-interacting systems.

The Hartree potential $v_H(\mathbf{r})$ is given by

$$v_H(\mathbf{r}) = \int d\mathbf{r}' \frac{\rho(\mathbf{r}')}{|\mathbf{r} - \mathbf{r}'|}. \tag{1.22}$$

The exchange-correlation potential $v_{xc}[\rho]$ is a functional derivative of the exchange-correlation energy with respect to the density evaluated at the ground-state density:

$$v_{xc}(\mathbf{r}) = \left. \frac{\delta E_{xc}[\rho]}{\delta \rho(\mathbf{r})} \right|_{\tilde{\rho}(\mathbf{r}) = \rho(\mathbf{r})}. \tag{1.23}$$

Looking upon the structure of the variational equation (1.20) it is evident that the same equation could have been written for a non-interacting system of electrons that experiences the external potential $v_{KS}(\mathbf{r})$. Consequently Kohn and Sham deduced that the ground-state density of the interacting system in question can be acquired by solving a set of single-particle Schrödinger equations describing a non-interacting system:

$$\left[-\frac{1}{2} \nabla^2 + v_{KS}(\mathbf{r}) \right] \phi_j(\mathbf{r}) = \varepsilon_j \, \phi_j(\mathbf{r}). \tag{1.24}$$

The density is constructed from the single particle orbitals as follows:

$$\rho(\mathbf{r}) = \sum_{i=1}^{N} |\phi_i(\mathbf{r})|^2. \tag{1.25}$$

Then we can express the ground-state energy in the following manner:

$$E_0[\rho] = -\sum_{i=1}^{N} \int d\mathbf{r} \, \phi_i^*(\mathbf{r}) \frac{\nabla^2}{2} \phi_i(\mathbf{r}) + \frac{1}{2} \int d\mathbf{r} d\mathbf{r}' \frac{\rho(\mathbf{r}) \, \rho(\mathbf{r}')}{|\mathbf{r} - \mathbf{r}'|} + \int d\mathbf{r} \, v_{ext} \, \rho(\mathbf{r}) + E_{xc}[\rho]. \tag{1.26}$$

Equations (1.24) and (1.25) with $v_{KS}(\mathbf{r})$ given by Eq. (1.21) are called the Kohn-Sham equations. They have to be solved self-consistently: Starting from a guess for the potential $v_{KS}(\mathbf{r})$ the single particle equations (1.24) are solved, the density is calculated using (1.25), and a new potential is constructed from Eqs. (1.21)-(1.23). The procedure is repeated until the density is sufficiently converged, *i.e.*, the change in the density between two consecutive self-consistency cycles is less than a predefined value.

It is important to note that the Kohn-Sham equations are exact - no approximations have been made during their derivation. All the many-body effects are preserved in the Kohn-Sham potential. However the exact expression for the exchange-correlation energy $E_{xc}[\rho]$, which yields the exchange-correlation potential is not known. By construction this term includes all non-classical electronic interactions such as the Pauli exclusion principle, electron correlation effects and the difference between the kinetic energy of the interacting system and the non-interacting one. In other words all the difficulties of the many-body problem are transferred to the exchange-correlation energy. The success of DFT in the Kohn-Sham formulation

hinges therefore on finding the most accurate approximation for $E_{xc}[\rho]$. The exact exchange-correlation energy has to obey a number of formal properties such as certain scaling relations, size consistency, functional derivative discontinuity.[4] Such properties can be used as guidelines for construction of suitable approximations, thus facilitating the search, or they can be used for testing the accuracy of a given approximation.

In the next section we will review some prominent approximations for $E_{xc}[\rho]$. We begin with LDA, the approximation being the most basic one, and continue with the ones employed in this thesis – GGA, and an exact-exchange-based hybrid approach.

1.4 Approximations for the exchange-correlation energy

1.4.1 The local-density approximation

The first and most simple approximation for exchange-correlation energy is the local-density approximation (LDA) and was devised by Kohn and Sham [5] in 1965. We can arrive at the expression for LDA by means of the following simplification. Assuming that the density of a given system is sufficiently slow varying we can think of this system as comprised of small volume elements $d\mathbf{r}$ each containing a homogeneous electron gas[5] described by a local density $\rho(\mathbf{r})$ at the coordinate $\mathbf{r}$. Then the exchange-correlation energy of one such volume element can be represented by the exchange-correlation energy per particle $e_{xc}(\rho(\mathbf{r}))$ times the particle number in the volume element $\rho(\mathbf{r})d\mathbf{r}$. Summing over all elements we get the exchange-correlation energy of the system:

$$E_{xc}[\rho] = \int d\mathbf{r}\, e_{xc}\left(\rho(\mathbf{r})\right)\rho(\mathbf{r}). \tag{1.27}$$

The exchange part of $e_{xc}(\rho(\mathbf{r}))$ is known analytically:

$$e_x(\rho(\mathbf{r})) = \frac{3k_F}{4\pi}, \tag{1.28}$$

with the Fermi wave vector

$$k_F = (3\pi^2 n)^{\frac{1}{3}}. \tag{1.29}$$

The exact expression for the correlation part is known only in the limit of extreme densities. To determine the correlation for arbitrary densities Quantum Monte Carlo simulations were performed by Ceperly and Alder [7] and their results were parametrized analytically (*e.g.* in [8, 9]).

The LDA is obviously exact for the homogeneous electron gas and close to exact for systems with slow-varying density such as metals, more precisely for systems

---

[4]For a thorough discussion of these properties see [6].

[5]A model system where an infinite number of electrons produces a constant density over space that is balanced by a uniform positive background.

where the variation of the density is small over distances given by the Fermi wavelength $2\pi/k_F$ [5].

Despite the fact that in many real systems this condition is not fulfilled, LDA turned out to produce astonishingly accurate results [10]. It yields bond lengths of molecules and geometries of solids to within 5% of accuracy though tending to underestimate them. Even systems with rapid density variations such as atoms and molecules are described better than originally expected - their ionization and dissociation energies agree to within $10\% - 20\%$ of the experimantal values. The reason for the success of LDA can be attributed to the fact that it exhibits many correct formal features such as correct coordinate scaling of the exchange and correlation parts, size consistency and the correct low-density behavior of the correlation energy [6].

Since the local-density approximation is computationally cheap and gives reliable results with known systematic errors like the overestimation of bonding strength, it is still widely used for electronic-structure calculations. Some shortcomings of LDA can be improved upon by the generalized gradient approximation.

1.4.2 The generalized gradient approximation

An extension of LDA is the so-called generalized gradient approximation (GGA) developed by Perdew and coworkers [11]. It goes beyond the local-density contribution as it takes into account spatial variations of the density, thus accounting for the inhomogeneity of the system:

$$E_{xc}^{\mathrm{GGA}}[\rho](\mathbf{r}) = \int f(\rho(\mathbf{r}), |\nabla\rho(\mathbf{r})|, ...) \, \rho(\mathbf{r})\mathrm{d}\mathbf{r}. \tag{1.30}$$

The GGA is known to improve structural properties of systems greatly differing from the uniform gas approximation such as molecules.

Various parametrizations of GGA exist that are constructed either by fitting of empirical parameters or by parameter-free considerations using known exact properties of the exchange-correlation functional. In this work, we use a GGA functional built with the latter method by Perdew, Burke, and Enzerhof [12]. We will refer to it as the PBE exchange-correlation functional.

1.4.3 A hybrid approach using exact exchange

Further efforts to find better approximations for E_{xc} has lead to potentials that treat the exchange part exactly as it is known analytically. This approach is especially attractive because the exact exchange (EXX) cancels out the self-interaction error, a classical effect stemming from the Hartree term that allows a spurious repulsion of the electron from itself. The LDA and GGA approximations do not account for this error thus resulting, *e.g.*, in inadequate treatment of localized orbitals (see discussion in [62]). In this work, we want to employ an exchange-correlation approximation which is partly based on such a method: A hybrid approach containing

a combination of the exact-exchange functional and the GGA functional.

Let us first look at the exact-exchange method. Evaluating the Kohn-Sham equations containing the exchange energy E_x is not straightforward. E_x is defined as follows:

$$E_x = -\frac{1}{2} \sum_{i,j}^N \int d\mathbf{r} \int d\mathbf{r}' \frac{\phi_i^*(\mathbf{r}) \phi_j(\mathbf{r}) \phi_j^*(\mathbf{r}') \phi_i(\mathbf{r}')}{|\mathbf{r} - \mathbf{r}'|}. \tag{1.31}$$

It depends explicitly on a set of occupied Kohn-Sham orbitals and therefore implicitly on the electron density. However to obtain the corresponding v_x one needs to know the explicit density dependent expression for E_x since the potential is defined as a functional derivative of E_x with respect to the density. In absence of a mapping between the orbitals and density other schemes need to be formulated.

The "Optimized Effective Potential" (OEP) method enables the evaluation of Eq. (1.31) and more generally of any orbital-dependent functional. Sharp and Horton [13] were the first to present the method on a Hartree-Fock-like expression before the emergence of DFT. It was later elaborated upon by Talman and Shadwick [14]. The method rests upon the principle of energy minimization. But instead of minimizing the total energy with respect to the density as in Eq. (1.13) a minimization with respect to the effective potential is performed with the total energy expressed in terms of Kohn-Sham orbitals:

$$\left. \frac{\delta E[\{\phi_i\}]}{\delta v_{KS}(\mathbf{r})} \right|_{v_{KS}=v^{\text{OEP}}} = 0. \tag{1.32}$$

Both approaches are equivalent since the Hohenberg-Kohn theorem guarantees a unique relationship between ρ and v_{KS}. Making use of the chain rule for functional derivatives one can further write

$$\sum_i^N \int d\mathbf{r}' \frac{\delta E[\{\phi_j\}]}{\delta \phi_i(\mathbf{r}')} \left. \frac{\delta \phi_i(\mathbf{r}')}{\delta v_{KS}(\mathbf{r})} \right|_{v_{KS}=v^{\text{OEP}}} + c.c. = 0. \tag{1.33}$$

The first derivative in Eq. (1.33) can be easily calculated using Eq. (1.26):

$$\frac{\delta E[\{\phi_i\}]}{\delta \phi_i(\mathbf{r}')} = \left(-\frac{1}{2} \nabla_{\mathbf{r}'}^2 + v_{ext}(\mathbf{r}') + v_H(\mathbf{r}') \right) \phi_i^*(\mathbf{r}') + \frac{\delta E_{xc}[\{\phi_i\}]}{\delta \phi_i(\mathbf{r}')}. \tag{1.34}$$

Using first-order perturbation theory we obtain an expression for the second derivative in the integrand of Eq. (1.33):

$$\frac{\delta \phi_i(\mathbf{r}')}{\delta v_{KS}(\mathbf{r})} = -\sum_{\substack{k=1 \\ k \neq i}}^\infty \frac{\phi_k^*(\mathbf{r}) \phi_i(\mathbf{r})}{\varepsilon_k - \varepsilon_i} \phi_k(\mathbf{r}'). \tag{1.35}$$

By inserting Eqs. (1.34) and (1.35) into (1.33) and rewriting the first summand of (1.34) with the help of Kohn-Sham equation (1.24) to include the exchange-

correlation potential the OEP integral equation is derived:

$$\sum_i^N \int d\mathbf{r}' \left[v_{xc}(\mathbf{r}') - u_{xc}(\mathbf{r}')\right] \left(\sum_{\substack{k=1 \\ k\neq i}}^\infty \frac{\phi_k^*(\mathbf{r})\,\phi_k(\mathbf{r}')}{\varepsilon_k - \varepsilon_i}\right) \phi_i(\mathbf{r})\,\phi_i^*(\mathbf{r}') + c.c. = 0, \qquad (1.36)$$

with

$$u_{xc}(\mathbf{r}) = \frac{1}{\phi_i^*(\mathbf{r})} \frac{\delta E_{xc}[\{\phi_j\}]}{\delta\phi_i(\mathbf{r})}, \qquad (1.37)$$

where a functional derivative of E_{xs} with respect to the orbitals is defined so that the expression (1.31) for the exact exchange can be used resolving the problem stated above.

However, the solution of the integral equation (1.36) is numerically very demanding. If solids are to be handled using OEP, additional approximations like that of Krieger, Li and Iafrate [15] have to be introduced. Because of these complications an alternative methodology for treating the exact exchange was developed by Görling [57]. It is based on an exact Kohn-Sham scheme derived with the help of perturbation theory by Görling and Levy [59]. As will be seen later the method can be converted into the OEP formalism but it has the advantage to be applicable to solids without the need for further approximations.

Starting directly with the definition of the exchange potential, a functional-derivative chain rule is applied twice:

$$\begin{aligned}
v_x[\rho] &= \frac{\delta E_x[\rho]}{\delta\rho(\mathbf{r})} \\
&= \sum_i^N \int d\mathbf{r}' \int d\mathbf{r}'' \left[\frac{\delta E_x}{\delta\phi_i(\mathbf{r}'')} \frac{\delta\phi_i(\mathbf{r}'')}{\delta v_{KS}(\mathbf{r}')} + \frac{\delta E_x}{\delta\phi_i^*(\mathbf{r}'')} \frac{\delta\phi_i^*(\mathbf{r}'')}{\delta v_{KS}(\mathbf{r}')}\right] \frac{\delta v_{KS}(\mathbf{r}')}{\delta\rho(\mathbf{r})}.
\end{aligned} \qquad (1.38)$$

In this manner the orbital dependence of E_x can be directly exploited. For the functional derivative $\delta E_x/\delta\phi_i(\mathbf{r})$ we obtain:

$$\frac{\delta E_x}{\delta\phi_i(\mathbf{r}'')} = \sum_l^N \int d\mathbf{r}' \frac{\phi_i^*(\mathbf{r}')\,\phi_l^*(\mathbf{r}'')\,\phi_l(\mathbf{r}')}{|\mathbf{r}' - \mathbf{r}''|}. \qquad (1.39)$$

For $\delta\phi_i(\mathbf{r}'')/\delta v_{KS}(\mathbf{r}')$ we use the result obtained from perturbation theory specified above in Eq. (1.35). The final term $v_{KS}(\mathbf{r})/\rho(\mathbf{r})$ occurring in Eq. (1.38) requires a more thorough discussion. By virtue of the Hohenberg-Kohn theorem it is legitimate to consider $v_{KS}(\mathbf{r})$ a functional of the density $\rho(\mathbf{r})$: it ensures the existence of a one-to-one mapping between the local potential of the system and its electron density to within an addition of a constant to the potential. The static linear-response operator $\hat{X}$ mediates this mapping by relating the reaction of the electron density $\rho(\mathbf{r})$ to infinitesimal changes of the potential $v_{KS}(\mathbf{r})$:

$$\delta\rho(\mathbf{r}) = \int d\mathbf{r}' X(\mathbf{r}, \mathbf{r}')\,\delta v_{KS}(\mathbf{r}'). \qquad (1.40)$$

Using the definition of the density $\rho(\mathbf{r}) = \sum_i^N \phi_i^*(\mathbf{r})\,\phi_i(\mathbf{r})$ and Eq. (1.35) we get a relation for $X(\mathbf{r}, \mathbf{r}')$:

$$
\begin{aligned}
X(\mathbf{r}, \mathbf{r}') = \frac{\delta\rho(\mathbf{r})}{\delta v_{KS}(\mathbf{r}')} &= \sum_i^N \int d\mathbf{r}'' \, \frac{\delta\rho(\mathbf{r})}{\delta\phi_i(\mathbf{r}'')} \frac{\delta\phi_i(\mathbf{r}'')}{\delta v_{KS}(\mathbf{r}')} + c.c. \\
&= \sum_i^N \sum_{\substack{j=1 \\ j \neq i}}^\infty \frac{\phi_i^*(\mathbf{r})\,\phi_j(\mathbf{r})\,\phi_j^*(\mathbf{r}')\,\phi_i(\mathbf{r}')}{\varepsilon_i - \varepsilon_j} + c.c..
\end{aligned}
\tag{1.41}
$$

Inversion of $X(\mathbf{r}, \mathbf{r}') = \delta\rho(\mathbf{r})/\delta v_{KS}(\mathbf{r}')$ should therefore give us the functional derivative $v_{KS}(\mathbf{r})/\rho(\mathbf{r})$. Direct inversion is, however, not possible due to the following problem: According to the Hohenberg-Kohn theorem an addition of a constant to the potential leaves the electron density unchanged. Constant functions are therefore eigenfunctions of $\hat{X}$ with zero eigenvalues. The problem can be sidestepped by representing $v_{KS}(\mathbf{r})$ and $\rho(\mathbf{r})$ within a finite basis set. In that case $\hat{X}$ can be inverted in a reduced basis set excluding the linear combinations of basis functions representing constant functions.

Summarizing, the following relation for the exchange potential is obtained:

$$
v_x(\mathbf{r}) = \int d\mathbf{r}' \left[\sum_i^N \sum_{\substack{k=1 \\ k \neq i}}^\infty \langle \phi_i | \hat{v}_x^{NL} | \phi_k \rangle \frac{\phi_k^*(\mathbf{r}')\,\phi_i(\mathbf{r}')}{\varepsilon_i - \varepsilon_k} + c.c. \right] \frac{\delta v_{KS}(\mathbf{r}')}{\delta\rho(\mathbf{r})},
\tag{1.42}
$$

containing the non-local exchange operator $\hat{v}_x^{NL}$ given by

$$
\langle \phi_i | \hat{v}_x^{NL} | \phi_k \rangle = \sum_l^N \int d\mathbf{r} \int d\mathbf{r}' \, \frac{\phi_i^*(\mathbf{r})\,\phi_l^*(\mathbf{r}')\,\phi_l(\mathbf{r})\,\phi_k(\mathbf{r}')}{|\mathbf{r}' - \mathbf{r}|}.
\tag{1.43}
$$

If we apply $\int d\mathbf{r}'' \, X(\mathbf{r}, \mathbf{r}'')$ on both sides of Eq. (1.42) the OEP relation Eq. (1.36) is reconstructed.

Knowing how to treat exact exchange, a hybrid method combining a fraction of it can be formulated. Here the following exchange-correlation functional that we will call PBE0$'$ is employed:

$$
E_{xc}^{\mathrm{PBE0}'}[\rho] = \alpha E_x + (1 - \alpha) E_x^{\mathrm{GGA}} + E_c^{\mathrm{GGA}},
\tag{1.44}
$$

with the mixing coefficient $\alpha = 0.25$.

To take a mixing coefficient close to 1 is disadvantageous because the exact exchange is, strictly speaking, incompatible with correlation functionals such as LDA or GGA. Utilizing a concept of an exchange-correlation hole one can observe a certain "cancellation of errors" taking place if both exchange and correlation part exhibit the same, *e.g.*, local, nature [6]. It is not present when a part of E_{xc} is highly non-local like the exact exchange and local or semilocal like the LDA or GGA functionals.

1.5 Interpretation of the Kohn-Sham eigenvalues and the band-gap problem

Density-functional theory as presented in Sections 1.2–1.3 aims at describing the ground-state properties of an interacting-electron system. The variational principle on which the proof of the Hohenberg-Kohn theorem is based applies solely to the ground state. However within this work we are particularly interested in the excited-state properties of a system like the electronic band structure, the band gap, and optical absorption. We want to examine the question whether some excited-state properties can nevertheless be obtained using DFT. Since the ground-state density fully determines the Hamiltonian of the system which, in turn, determines the excited-state properties, these should in principle be accessible through the ground-state density [58]. However no practical scheme exists to link the excited-state quantities to the density.

Let us consider the Kohn-Sham eigenvalues ε_i. It is customary to interpret them as the electronic band structure of the system, even though they were introduced as mathematical devices, Lagrange multipliers, with no physical meaning. This interpretation proved to be successful but for one important limitation: The Kohn-Sham band gap of insulators and semiconductors was found to be about 50% smaller compared to their experimentally determined fundamental band gap. This was often attributed to the failure of the local or semilocal approximations to the exchange-correlation potential, however the problem lies within the Kohn-Sham approach itself as shown in the following.

The fundamental band gap $E_g(N)$ of an N electron system is defined as the difference between the ionization potential $I(N)$ and the electron affinity $A(N)$

$$E_g(N) = I(N) - A(N) \tag{1.45}$$

which, in turn, are defined as single-electron removal and addition energies, respectively,

$$
\begin{aligned}
I(N) &= E_{N-1}^{(0)} - E_N^{(0)} \\
A(N) &= E_N^{(0)} - E_{N+1}^{(0)}
\end{aligned}
\tag{1.46}
$$

with $E_N^{(0)}$ denoting the ground state of the N electron system. The band gap is therefore expressed using ground-state energy differences of $N-1$, N and $N+1$ systems.

It is also possible to express the band gap through Kohn-Sham eigenvalues by applying Janak's theorem [16]. It states that the ith occupied eigenvalue is equal to the partial derivative of the total energy with respect to the fractional occupation of ith orbital. It can be shown [17, 18] that, following this theorem, only the eigenvalue $\varepsilon_N(N)$ corresponding to the highest occupied orbital has a rigorous physical

meaning[6], namely:

$$\varepsilon_N(N) = -I(N). \qquad (1.47)$$

Since the electron affinity of an N electron system is equal to the ionization potential of the $N + 1$ electron system (see Eq. (1.46)) $A(N) = I(N + 1)$ the band gap can be expressed as follows using Eq. (1.47)

$$E_g(N) = I(N) - I(N + 1) = \varepsilon_{N+1}(N + 1) - \varepsilon_N(N). \qquad (1.48)$$

Now we examine the Kohn-Sham band gap of the non-interacting electron system. It is obviously the difference between the energies of the lowest unoccupied and the highest occupied orbitals:

$$E_g^{KS}(N) = \varepsilon_{N+1}(N) - \varepsilon_N(N). \qquad (1.49)$$

Combining Eqs. (1.48) and (1.49) we obtain a relation between the actual band gap and the Kohn-Sham one:

$$E_g(N) = E_g^{KS}(N) + (\varepsilon_{N+1}(N + 1) - \varepsilon_{N+1}(N)) = E_g^{KS}(N) + \Delta_{xc}. \qquad (1.50)$$

Thus we see that the actual fundamental band gap differs from the Kohn-Sham gap by a rigid shift denoted by Δ_{xc} which constitutes the difference between the lowest unoccupied orbitals of the neutral N and ionized $N + 1$ systems. We can analyze which part of the Kohn-Sham scheme engenders this shift. The addition of an extra electron in an extended solid with $N \gg 0$ causes only an infinitesimal change in the electron density. Hence the external potential is in effect the same for the N and $N - 1$ electron systems. Since the Hartree potential depends explicitly on the density, it does not change either. The rigid shift Δ_{xc} has to be therefore generated entirely by the exchange-correlation potential. It is a well known property of the exchange-correlation potential and is referred to as its derivative discontinuity: An infinitesimal change in the density gives rise to a finite change in the exchange-correlation potential

$$\Delta_{xs} = \left. \frac{\delta E_{xc}[\rho]}{\delta \rho(\mathbf{r})} \right|_{N+1} - \left. \frac{\delta E_{xc}[\rho]}{\delta \rho(\mathbf{r})} \right|_N. \qquad (1.51)$$

The underestimation of the band gap is thus an inherent characteristic of the Kohn-Sham scheme. The size of the discontinuity is dependent on the system in question. In addition, the use of an approximate exchange-correlation functional introduces further errors. Several studies [19, 20] showed that for typical semiconductors and insulators the derivative discontinuity accounts for 80% of the band gap error using LDA. To obtain correct excitation spectra we have to go beyond DFT and employ methodologies based on the many-body perturbation theory. The main concepts of these methods are presented in the next chapter.

---

[6]We denote the ith Kohn-Sham orbital of an N electron system by $\varepsilon_i(N)$.

Chapter 2

Many-body perturbation theory

2.1 Introduction

We have briefly shown in the previous chapter that DFT cannot provide us with excited-state properties of systems. A theoretically rigorous albeit computationally heavy way to calculate them is given by many-body perturbation theory (MBPT). In principle, we are interested in two qualitatively different types of excited-state properties.

The first are the single-particle excitation spectra. These are directly linked to direct photoemission and inverse photoemission experiments that are used to determine the band structure of a system. Within the former, an electron is extracted from a solid in the ground state by means of a photon impinging on the system. The corresponding occupied energy level is determined from the energy of the electron. Within the latter, an electron is absorbed into the solid, and by measuring the energy of the ejected photon the unoccupied states are found. Thus, we deal with excited states of the solid containing $N-1$ and $N+1$ electrons respectively. So if a theoretical scheme is to be applied for the calculation of such single-particle spectra it has to permit the variation of the electron number. As we will see, Green function theory is the natural way to approach this problem. The solution of the equation of motion for the one-particle Green function, determines the single-particle excitation spectrum.

The second type of excited-state properties we are interested in are neutral excitations that are probed in optical absorption experiments. The absorption of a photon does not cause the emission of the electron, instead the system evolves to an excited state with the electron occupying an energetically higher state and possibly interacting with the remaining hole. The process is described by the formation of electron-hole pairs also called excitons. These two-particle effects are captured by the two-particle Green function. Its equation of motion, the Bethe-Salpeter equation, is used to determine the exciton spectrum.

In this chapter we shall outline the Green function formalism following the discussions in the works by Fetter and Walecka [21] and Strinati [22]. The first part of the presentation will lead to a method for obtaining the single-particle excitation

spectrum of materials - the G_0W_0 approximation. The second part will concentrate on the electron-hole excitations. The G_0W_0 results as well as the electron-hole excitations shall be incorporated in the derivation of the macroscopic dielectric function which describes optical absorption spectra.

2.2 Single-particle excitations

2.2.1 Green functions

For the following discussion of the Green-functions method the language of second quantization is most suited. So let us reformulate the many-body problem represented by the Hamiltonian (1.2) within this formalism. To that end let us first rewrite Eq. (1.2) in a way that distinguishes the single- and two-particle contributions:

$$\hat{H} = \sum_i \hat{h}(\mathbf{r}_i) + \frac{1}{2} \sum_{i \neq j} v(\mathbf{r}_i, \mathbf{r}_j). \tag{2.1}$$

The single-particle term

$$\hat{h}(\mathbf{r}) = -\frac{1}{2}\nabla^2 + \sum_I \frac{Z_I}{|\mathbf{r} - \mathbf{R}_I|} \tag{2.2}$$

contains the kinetic energy of the electrons and the electrostatic interaction of the electrons with the nuclei. The demanding two-particle term describes the electron-electron interaction:

$$v(\mathbf{r}, \mathbf{r}') = \frac{1}{\mathbf{r} - \mathbf{r}'}. \tag{2.3}$$

In second quantization, Eq. (2.1) is expressed with the help of field operators $\hat{\psi}(\mathbf{r})$ and $\hat{\psi}^\dagger(\mathbf{r})$ that annihilate and create an electron at the position $\mathbf{r}$, respectively. In case of fermions – as considered here – they obey the anti-commutation relations

$$\{\hat{\psi}(\mathbf{r}), \hat{\psi}^\dagger(\mathbf{r}')\} = \delta(\mathbf{r} - \mathbf{r}'),$$
$$\{\hat{\psi}(\mathbf{r}), \hat{\psi}(\mathbf{r}')\} = \{\hat{\psi}^\dagger(\mathbf{r}), \hat{\psi}^\dagger(\mathbf{r}') = 0. \tag{2.4}$$

The many-body Hamiltonian then assumes the following form:

$$\hat{H} = \int d\mathbf{r}\, \hat{\psi}^\dagger(\mathbf{r})\, \hat{h}(\mathbf{r})\, \hat{\psi}(\mathbf{r}) + \frac{1}{2} \int d\mathbf{r} d\mathbf{r}'\, \hat{\psi}^\dagger(\mathbf{r})\, \hat{\psi}^\dagger(\mathbf{r}')\, v(\mathbf{r}, \mathbf{r}')\, \hat{\psi}(\mathbf{r}')\, \hat{\psi}(\mathbf{r}). \tag{2.5}$$

Formulating the time-evolution of the field operators in the Heisenberg picture as

$$\hat{\psi}(\mathbf{r}, t) = e^{i\hat{H}t}\, \hat{\psi}(\mathbf{r})\, e^{-i\hat{H}t} \tag{2.6}$$

we are now able to define the one-particle Green function:

$$G(\mathbf{r}, t, \mathbf{r}', t') = -i\, \langle \Psi_N^{(0)} | \mathcal{T}[\hat{\psi}(\mathbf{r}, t)\, \hat{\psi}^\dagger(\mathbf{r}', t')] | \Psi_N^{(0)} \rangle. \tag{2.7}$$

Here $|\Psi_N^{(0)}\rangle$ indicates the normalized ground state of an N electron system. $\mathcal{T}$ is the Wick time-ordering operator, which orders a product of time-dependent operators from left to right according to decreasing time, with each corresponding permutation of the (fermion) field operators producing a minus sign:

$$\mathcal{T}[\hat{\psi}(\mathbf{r},t)\,\hat{\psi}^\dagger(\mathbf{r}',t')] = \begin{cases} \hat{\psi}(\mathbf{r},t)\,\hat{\psi}^\dagger(\mathbf{r}',t'), & t > t' \\ -\hat{\psi}^\dagger(\mathbf{r}',t')\,\hat{\psi}(\mathbf{r},t), & t < t'. \end{cases} \tag{2.8}$$

The Green function can be defined for any number of particles by extending the definition (2.7) to include the creation and annihilation operators for each particle. Apart from the one-particle Green function we are interested in the two-particle Green function since it will be central to the discussion of electron-hole pairs. The two-particle Green function is defined as

$$\begin{aligned} G_2&(\mathbf{r}_1,t_1,\mathbf{r}_2,t_2;\mathbf{r}_1',t_1',\mathbf{r}_2',t_2') \\ &= -\langle\Psi_N^{(0)}|\mathcal{T}[\hat{\psi}(\mathbf{r}_1,t_1)\,\hat{\psi}(\mathbf{r}_2,t_2)\,\hat{\psi}^\dagger(\mathbf{r}_2',t_2')\,\hat{\psi}^\dagger(\mathbf{r}_1',t_1')]|\Psi_N^{(0)}\rangle. \end{aligned} \tag{2.9}$$

Let us now consider the physical meaning of the (one-particle) Green function. The physically intuitive interpretation of $G(\mathbf{r},t,\mathbf{r}',t')$ is given by its definition. For the case $t > t'$ $G(\mathbf{r},t,\mathbf{r}',t')$ expresses the probability that an electron added to the system at position $\mathbf{r}'$ and time t' is found at the position $\mathbf{r}$ at a later time t. For $t < t'$ $G(\mathbf{r},t,\mathbf{r}',t')$ is the probability that a hole created at position $\mathbf{r}$ and time t travels to $\mathbf{r}'$ at time t'. So the one-particle Green function describes the propagation of an added or removed particle through time - the processes happening in direct and inverse photoemission experiments.

Writing the Green function in the so-called Lehmann or spectral representation will clarify how excitation energies of the system are connected to the Green function [21]. To obtain the Lehmann representation, we first insert the closure relation of eigenstates $|\Psi_{N+1}^{(n)}\rangle$ $\left(|\Psi_{N-1}^{(n)}\rangle\right)$ corresponding to an excited system with $N+1$ ($N-1$) electrons between the field operators for the case $t > t'$ ($t < t'$). Extracting the time dependence of the field operators by applying the eigenvalue equation

$$\hat{H}\,|\Psi_N^{(n)}\rangle = E_N^{(n)}\,|\Psi_N^{(n)}\rangle \tag{2.10}$$

we obtain:

$$G(\mathbf{r},t,\mathbf{r}',t') =$$
$$\begin{cases} -i\sum_n e^{-i\left[E_{N+1}^{(n)}-E_N^{(0)}\right](t-t')}\langle\Psi_N^{(0)}|\hat{\psi}(\mathbf{r})|\Psi_{N+1}^{(n)}\rangle\langle\Psi_{N+1}^{(n)}|\hat{\psi}^\dagger(\mathbf{r}')|\Psi_N^{(0)}\rangle, & t > t' \\ +i\sum_n e^{-i\left[E_N^{(0)}-E_{N-1}^{(n)}\right](t-t')}\langle\Psi_N^{(0)}|\hat{\psi}^\dagger(\mathbf{r}')|\Psi_{N-1}^{(n)}\rangle\langle\Psi_{N-1}^{(n)}|\hat{\psi}(\mathbf{r})|\Psi_N^{(0)}\rangle, & t < t'. \end{cases} \tag{2.11}$$

Performing a Fourier transform with respect to $t - t'$ leads to the Lehmann repre-

sentation in frequency space

$$G(\mathbf{r}, \mathbf{r}'; \omega) = \sum_n \frac{\psi_n(\mathbf{r})\, \psi_n^*(\mathbf{r}')}{\omega - \mathcal{E}_n - i\eta\, \mathrm{sgn}(\mu - \mathcal{E}_n)}, \tag{2.12}$$

where

$$
\begin{aligned}
\psi_n(\mathbf{r}) &= \langle \Psi_N^{(0)} | \hat{\psi}(\mathbf{r}) | \Psi_{N+1}^{(n)} \rangle\,, \quad &\mathcal{E}_n &= E_{N+1}^{(n)} - E_N^{(0)}, \quad &\text{if} \quad \mathcal{E}_n > \mu \\
\psi_n(\mathbf{r}) &= \langle \Psi_{N-1}^{(n)} | \hat{\psi}(\mathbf{r}) | \Psi_N^{(0)} \rangle\,, \quad &\mathcal{E}_n &= E_N^{(0)} - E_{N-1}^{(n)}, \quad &\text{if} \quad \mathcal{E}_n < \mu.
\end{aligned}
\tag{2.13}
$$

μ denotes the chemical potential. The introduction of the term $i\eta$ with $\eta \to 0^+$ is necessary to ensure the convergence of the time integral.

We see that $\mathcal{E}_n$ - the poles of the Green function - correspond precisely to the nth excitation energies of the system due to the addition or removal of a particle. The excitation energies can be computed directly by solving the Dyson equation – the reformulated equation of motion for the one-particle Green function. The next section shall be devoted to the derivation of the Dyson equation following mainly the presentation in Strinati [22].

2.2.2 Dyson equation

The equation of motion for the one-particle Green function can be obtained by evaluating $\partial G(\mathbf{r}, t, \mathbf{r}', t')/\partial t$. To that end we first calculate the equation of motion for the field operator $\hat{\psi}(\mathbf{r}, t)$ with the help of the anti-commutation relations (2.4):

$$i\frac{\partial}{\partial t}\hat{\psi}(\mathbf{r}, t) = [\hat{\psi}(\mathbf{r}, t), \hat{H}] = \left[\hat{h}(\mathbf{r}) - \int d\mathbf{r}'\, v(\mathbf{r}, \mathbf{r}')\, \hat{\psi}^\dagger(\mathbf{r}', t)\, \hat{\psi}(\mathbf{r}', t) \right] \hat{\psi}(\mathbf{r}, t). \tag{2.14}$$

While evaluating $\partial G(\mathbf{r}, t, \mathbf{r}', t')/\partial t$ using the above equation a term containing four field operators emerges that is identified as the two-particle Green function G_2:

$$
\begin{aligned}
\left[i\frac{\partial}{\partial t_1} - \hat{h}(\mathbf{r}_1) \right] G(\mathbf{r}_1, t_1, \mathbf{r}_1', t_1') &= \delta(\mathbf{r}_1 - \mathbf{r}_1')\, \delta(t_1 - t_1') \\
&\quad - i \int d\mathbf{r}_2\, dt_2\, v(\mathbf{r}_1, \mathbf{r}_2)\, \delta(t_1 - t_2)\, G_2(\mathbf{r}_1, t_1, \mathbf{r}_2, t_2; \mathbf{r}_1', t_1', \mathbf{r}_2', t_2'^+).
\end{aligned}
\tag{2.15}
$$

The notation t^+ indicates an infinitesimally larger time than t: $t^+ = \lim_{\eta \to 0^+}(t + \eta)$. It allows us to employ the time-ordering operator as $\mathcal{T}$ cannot be applied to a product of operators acting at equal times.

The presence of the two-particle Green function in the equation of motion for the one-particle Green function is rather unfortunate: If we try to grasp G_2 by means of the same approach - evaluating its equation of motion - we will find that it is coupled to the three-particle Green function. In general, Mattuck and Theumann [23] showed that the equation of motion for the N particle Green function involves the $N+1$ particle Green function. That means we would have to solve a hierarchy of

coupled differential equations gaining us no advantages over the original formulation of the many-body problem. There is however a way to bypass this problem. The functional derivative technique by Schwinger [24], Martin and Schwinger [25] and Kadanoff and Baym [26, 27] allows to express the two-particle Green function by a combination of terms depending on a one-particle Green function thus effectively decoupling the equations of motion.

In order to achieve this, we introduce an external perturbation $U_{ext}(\mathbf{r}, \mathbf{r}'; t)$. It is in general defined to be nonlocal in spatial coordinates, local in time and to vanish for $|t| \to \infty$. We will use it only as a tool to sidestep the problem of coupled equations of motion, and it will vanish at the end of the whole procedure. We can use the interaction picture to define the perturbation Hamiltonian:

$$\hat{H}'(t) = \int \mathrm{d}\mathbf{r}\mathrm{d}\mathbf{r}' \, \hat{\psi}^\dagger(\mathbf{r}, t^+) \, U_{ext}(\mathbf{r}, \mathbf{r}'; t) \, \hat{\psi}(\mathbf{r}', t). \tag{2.16}$$

Then the so-called generalized one-particle Green function describing the perturbed system is defined as follows:

$$G(\mathbf{r}, t, \mathbf{r}', t') = -i \frac{\langle \Psi_N^{(0)} | \mathcal{T}[\hat{S} \, \hat{\psi}(\mathbf{r}, t) \, \hat{\psi}^\dagger(\mathbf{r}', t')] | \Psi_N^{(0)} \rangle}{\langle \Psi_N^{(0)} | \mathcal{T}[\hat{S}] | \Psi_N^{(0)} \rangle}. \tag{2.17}$$

The operator $\hat{S}$ contains the external potential in the form

$$\hat{S} = \exp\left[-i \int_{-\infty}^{\infty} \mathrm{d}t \, \hat{H}'(t) \right], \tag{2.18}$$

so that for the case $U_{ext}(\mathbf{r}, \mathbf{r}'; t) = 0$ we return to the original definition of the one-particle Green function.

We obtain the equation of motion for the generalized one-particle Green function that at this stage contains the two-particle Green function:

$$\left[i \frac{\partial}{\partial t_1} - \hat{h}(1) \right] G(1, 2)$$
$$= \delta(1, 2) + \int \mathrm{d}(3) \, U_{ext}(1, 3) \, G(3, 2) - i \int \mathrm{d}(3) \, v(1, 3) \, G_2(1, 3; 2, 3^+). \tag{2.19}$$

To bring the notation in a more readable form we abbreviate different sets of coordinates $(\mathbf{r}_i, t_i)$ by their index (i), the integrals over these both coordinates are denoted by $\mathrm{d}(i)$ analogously. This coordinate index notation is also used for the following special terms:

$$\begin{aligned} \hat{h}(\mathbf{r}_i) &\to \hat{h}(i), \\ v(\mathbf{r}_i, \mathbf{r}_j) \, \delta(t_i - t_j) &\to v(i, j), \\ U_{ext}(\mathbf{r}_i, \mathbf{r}_j, t_i) \, \delta(t_i - t_j) &\to U_{ext}(i, j), \\ \delta(\mathbf{r}_i - \mathbf{r}_j) \, \delta(t_i - t_j) &\to \delta(i, j). \end{aligned} \tag{2.20}$$

Evaluating the first-order variation of $G(1,2)$ with respect to $U_{ext}(3,4)$ we obtain the functional derivative

$$\frac{\delta G(1,2)}{\delta U_{ext}(3,4)} = -G_2(1,4;2,3^+) + G(1,2)\,G(4,3^+) \qquad (2.21)$$

that lets us dispose of the two-particle Green function in Eq. (2.19). Assuming in the following a local perturbation potential

$$U_{ext}(1,2) = U_{ext}(1)\,\delta(1,2), \qquad (2.22)$$

the equation of motion (2.19) becomes

$$\left[i\frac{\partial}{\partial t_1} - \hat{h}(1) - U_{ext}(1)\right] G(1,2)$$
$$= \delta(1,2) - i\int d(3)\,v(1,3)\left[G(1,2)\,G(3,3^+) - \frac{\delta G(1,2)}{\delta U_{ext}(3)}\right]. \qquad (2.23)$$

For the benefit of later considerations we will rearrange some terms in the above equation. Let us define a local potential $V(1)$

$$V(1) = U_{ext}(1) - i\int d(3)\,v(1,3)\,G(3,3^+) \qquad (2.24)$$

that will enable us to replace references to the external perturbation $U_{ext}(1)$ later on. Noting that the electron density can be expressed by a Green function in the following way

$$\rho(1) = -i\,G(1,1^+), \qquad (2.25)$$

we see that the second term in Eq. (2.24) corresponds to the Hartree potential $v_H(1)$.

The equation of motion assumes then the form

$$\left[i\frac{\partial}{\partial t_1} - \hat{h}(1) - V(1)\right] G(1,2) = \delta(1,2) - i\int d(3)\,v(1,3)\,\frac{\delta G(1,2)}{\delta U_{ext}(3)}. \qquad (2.26)$$

Using the inverse of the Green function G^{-1} defined by the identity

$$\int d(4)\,G(1,4)\,G^{-1}(4,5) = \delta(1,5), \qquad (2.27)$$

we can write the functional derivative of $G(1,2)$ with respect to $U_{ext}(3)$ in a different way. By varying Eq. (2.27) with respect to $U_{ext}(3)$, multiplying it with $G(5,2)$ and integrating over the variable (5) we obtain the following functional derivative identity:

$$\frac{\delta G(1,2)}{\delta U_{ext}(3)} = -\int d(4,5)\,G(1,4)\,\frac{\delta G^{-1}(4,5)}{\delta U_{ext}(3)}\,G(5,2). \qquad (2.28)$$

Inserting this relation into the equation of motion we finally obtain the Dyson equation in its differential form

$$\left[i\frac{\partial}{\partial t_1} - \hat{h}(1) - V(1)\right] G(1,2) - \int d(3)\, \Sigma(1,3)\, G(3,2) = \delta(1,2), \qquad (2.29)$$

where we have introduced an operator that will be central to the following discussion, the self-energy operator:

$$\Sigma(1,2) = -i \int d(3,4)\, v(1,3)\, G(1,4)\, \frac{\delta G^{-1}(4,2)}{\delta U_{ext}(3)}. \qquad (2.30)$$

Let us illustrate the physical meaning of Σ by reformulating the Dyson equation as a quasi-particle equation. First a Fourier transform is performed to write Eq. (2.29) in frequency domain:

$$\left[\omega - \hat{h}_0(\mathbf{r})\right] G(\mathbf{r}, \mathbf{r}', \omega) - \int d\mathbf{r}''\, \Sigma(\mathbf{r}, \mathbf{r}'', \omega)\, G(\mathbf{r}'', \mathbf{r}') = \delta(\mathbf{r}, \mathbf{r}'), \qquad (2.31)$$

with

$$\hat{h}_0(\mathbf{r}) = \hat{h}(\mathbf{r}) + V(\mathbf{r}). \qquad (2.32)$$

Combining Eq. (2.31) with the spectral formulation of the Green function (2.12) we obtain the quasi-particle equation:

$$\hat{h}_0(\mathbf{r})\, \psi_i^{qp}(\mathbf{r}) - \int d\mathbf{r}'\, \Sigma(\mathbf{r}, \mathbf{r}'; \mathcal{E}_i^{qp})\, \psi_i^{qp}(\mathbf{r}') = \mathcal{E}_i^{qp}\, \psi_i^{qp}(\mathbf{r}). \qquad (2.33)$$

with the Lehmann amplitudes $\psi_n(\mathbf{r})$ denoted by $\psi_i^{qp}(\mathbf{r})$ and the excitation energies $\mathcal{E}_n$ denoted by $\mathcal{E}_i^{qp}$. The quasi-particle equation is a Schrödinger-like equation with Lehmann amplitudes as its eigenfunctions and the single-particle excitation energies as its eigenvalues. The operator $\hat{h}_0$ describes a non-interacting system subjected to an external and the Hartree potential.[1] All the many-body exchange and correlation effects are contained in the self-energy which acts as a non-local, energy-dependent single-particle potential. The self-energy is in general non-Hermitian so that the eigenvalues $\mathcal{E}_i^{qp}$ are complex. This fact is taken into account in the Lehmann representation of the Green function by performing an analytic continuation, *i.e.*, extending all quantities from the real frequency axis to the complex plane. Then the real part of an eigenvalue $\mathcal{E}_i^{qp}$ constitutes the single-particle excitation energy and the imaginary part reflects the finite lifetime of the excitation.

It is now apparent that we have reduced the initial problem to having to find an expression for the self-energy that determines the quasi-particle spectrum by means of the Dyson equation. In particular we want to find a scheme that eliminates explicit references to the external perturbation $U_{ext}(\mathbf{r})$. Such a procedure was proposed by Hedin in 1965 [28, 29] and will be sketched in the next section.

---

[1]The external perturbation $U_{ext}(\mathbf{r})$ that is still included in $\hat{h}_0$ will be eliminated in the next section.

2.2.3 Hedin equations

Hedin developed a set of coupled equations that yield the exact self-energy when solved self-consistently. The complete derivation is based on functional derivative techniques and can be found in [28, 29]. We restrict ourselves to discussion of the results, namely the five coupled equations:

$$G(1,2) = G_0(1,2) + \int d(3,4)\, G_0(1,3)\, \Sigma(3,4)\, G(4,2), \tag{2.34}$$

$$\Sigma(1,2) = i \int d(3,4)\, G(1,4)\, W(1^+,3)\, \tilde{\Gamma}(4,2;3), \tag{2.35}$$

$$W(1,2) = v(1,2) + \int d(3,4)\, v(1,3)\, \tilde{\chi}(3,4)\, W(4,2), \tag{2.36}$$

$$\tilde{\Gamma}(1,2;3) = \delta(1,2)\,\delta(1,3) + \int d(4,5,6,7)\, \frac{\delta\Sigma(1,2)}{\delta G(4,5)}\, G(4,6)\, G(7,5)\, \tilde{\Gamma}(6,7;3), \tag{2.37}$$

$$\tilde{\chi}(1,2) = -i \int d(3,4)\, G(2,3)\, G(4,2)\, \tilde{\Gamma}(3,4;1). \tag{2.38}$$

Let us clarify where the newly introduced quantities come from.

G_0 denotes the single-particle Green function corresponding to a non-interacting system on a Hartree level, *i.e.*, if the self-energy is set to zero:

$$\left[i\frac{\partial}{\partial t_1} - \hat{h}_0(1) \right] G_0(1,2) = \delta(1,2). \tag{2.39}$$

By means of this definition, the Dyson equation is reformulated in integral form resulting in Eq. (2.34).

$\tilde{\chi}$ is the irreducible polarizability that expresses the variation of the density ρ upon a variation of the total potential V:

$$\tilde{\chi}(1,2) = \frac{\delta\rho(1)}{\delta V(2)} = -i\,\frac{\delta G(1,1^+)}{\delta V(2)}. \tag{2.40}$$

At this point we also introduce the reducible polarizability χ that will be important for the discussion of the Bethe-Salpeter equation. χ relates the variation of the density ρ to the variation of the external potential U_{ext}:

$$\chi(1,2) = \frac{\delta\rho(1)}{\delta U_{ext}(2)} = -i\,\frac{\delta G(1,1^+)}{\delta U_{ext}(2)}. \tag{2.41}$$

The vertex function $\tilde{\Gamma}$ is defined by

$$\tilde{\Gamma}(1,2,3) = -\frac{\delta G^{-1}(1,2)}{\delta V(3)}. \tag{2.42}$$

The iterative solution of Hedin equations corresponds to a perturbative expansion of the self-energy in terms of the dynamical screened Coulomb interaction W. This

quantity can be understood as the reduced Coulomb interaction between electrons in a medium - it arises because of the fact that the bare Coulomb interaction $v(1,2)$ is screened due to the presence of other electrons in the system. The interaction is called 'dynamical' because it exhibits a frequency dependence as opposed to $v(1,2)$ which is static. The screening effect is described by the inverse microscopic dielectric function ϵ^{-1} that is defined as the change of the total potential V with respect to changes in the external potential U_{ext}:

$$\epsilon^{-1}(1,2) = \frac{\delta V(1)}{\delta U_{ext}(2)}. \tag{2.43}$$

Then the dynamical screened Coulomb interaction is defined by:

$$W(1,2) = \int d(3)\, \epsilon^{-1}(1,3)\, v(3,2). \tag{2.44}$$

Starting from these definitions, manipulations employing functional derivative techniques yield the self-consistent set of equations as presented in [28, 22]. As the equations do not include references to the external perturbation, the limit $U_{ext} \to 0$ can be safely taken.

The iterative solution of Hedin equations is generally not attempted since it would be very involved computationally. Instead there exist various approaches with different levels of self-consistency. The one we are interested in is the so-called called $G_0 W_0$ approximation.

2.2.4 $G_0 W_0$ approximation

The $G_0 W_0$ approximation amounts to stopping the self-consistent procedure after one iteration, $i.e.$, considering the first order of the self-energy expansion in W. In detail, the following steps are carried out: Starting from $\Sigma = 0$, the Green function is equal to the non-interacting one. The second, complicated part of the vertex function is neglected leaving only a product of two delta functions. Then $\tilde{\Gamma}^0$ reduces the polarizability to a product of two Green functions in what is called the Random-Phase Approximation. Subsequently, the screened Coulomb interaction is calculated. At the end of this cycle the self-energy is calculated as a product of the Green function G_0 and and the screened Coulomb interaction W_0 giving rise to the name of the approximation. The resulting equations are summarized below:

$$G(1,2) = G_0(1,2), \tag{2.45}$$

$$\tilde{\Gamma}^0(1,2;3) = \delta(1,2)\,\delta(1,3), \tag{2.46}$$

$$\tilde{\chi}_0(1,2) = -i\, G_0(2,1)\, G_0(1,2), \tag{2.47}$$

$$W_0(1,2) = v(1,2) + \int d(3,4)\, v(1,3)\, \tilde{\chi}_0(3,4)\, W_0(4,2), \tag{2.48}$$

$$\Sigma(1,2) = i\, G_0(1,2)\, W_0(1^+,2). \tag{2.49}$$

The formalism suggests to use the independent-particle Green function on a Hartree level as a starting point. However, in practice a better choice for G_0 is obtained

from the Kohn-Sham calculations. To construct G_0 we can then make use of the Lehmann representation substituting the quasi-particle quantities $\phi_n(\mathbf{r})$ and ε_n by the respective Kohn-Sham ones:

$$G_0(\mathbf{r}, \mathbf{r}'; \omega) = \sum_n \frac{\phi_n(\mathbf{r})\, \phi_n^*(\mathbf{r}')}{\omega - \varepsilon_n - i\eta\, \mathrm{sgn}(\mu - \varepsilon_n)}. \tag{2.50}$$

Furthermore, Hybertsen and Louie [30] assumed that the single-particle orbitals and energies obtained from the Kohn-Sham calculations are good zeroth order approximations to the quasi-particle quantities. For simple materials like silicon it was shown that the Kohn-Sham orbitals are in very good agreement with the quasi-particle ones [31]. Then the solution of the full quasi-particle equation (2.33) is avoided by considering G_0W_0 eigenvalues as a first-order correction to the Kohn-Sham ones:

$$\mathcal{E}_i^{qp} = \varepsilon_i + \Re\, \langle \phi_i(\mathbf{r}) | \Sigma(\mathbf{r}, \mathbf{r}'; \mathcal{E}_i^{qp}) - v_{xc}(\mathbf{r})\, \delta(\mathbf{r} - \mathbf{r}') | \phi_i(\mathbf{r}') \rangle, \tag{2.51}$$

where the notation $\langle \phi_i(\mathbf{r}) | \hat{A}(\mathbf{r}, \mathbf{r}') | \phi_i(\mathbf{r}') \rangle$ indicates the expectation value of an operator $\hat{A}(\mathbf{r}, \mathbf{r}')$:

$$\langle \phi_i(\mathbf{r}) | \hat{A}(\mathbf{r}, \mathbf{r}') | \phi_i(\mathbf{r}') \rangle = \int d\mathbf{r} \int d\mathbf{r}' \phi_i^*(\mathbf{r}) A(\mathbf{r}, \mathbf{r}') \phi_i(\mathbf{r}'). \tag{2.52}$$

Because of the dependence of the self-energy on the quasi-particle energy we can not evaluate Eq. (2.51) directly. The issue is treated by expanding the self-energy around the Kohn-Sham energies up to the linear term:

$$\Sigma(\mathbf{r}, \mathbf{r}'; \mathcal{E}_i^{qp}) = \Sigma(\mathbf{r}, \mathbf{r}'; \varepsilon_i) + (\mathcal{E}_i^{qp} - \varepsilon_i) \left. \frac{\partial \Sigma(\mathbf{r}, \mathbf{r}'; \omega)}{\partial \omega} \right|_{\omega = \varepsilon_i} + \mathcal{O}[(\mathcal{E}_i^{qp} - \varepsilon_i)^2]. \tag{2.53}$$

Inserting this linearization in Eq. (2.51) and rearranging the terms we obtain the final expression for the quasi-particle energies:

$$\mathcal{E}_i^{qp} = \varepsilon_i + Z_i\, \Re\, \langle \phi_i(\mathbf{r}) | \Sigma(\mathbf{r}, \mathbf{r}'; \varepsilon_i) - v_{xc}(\mathbf{r})\, \delta(\mathbf{r} - \mathbf{r}') | \phi_i(\mathbf{r}') \rangle, \tag{2.54}$$

with the renormalization factor Z_i given by

$$Z_i = \left[1 - \Re\, \left. \frac{\partial\, \langle \phi_i(\mathbf{r}) | \Sigma(\mathbf{r}, \mathbf{r}'; \omega) | \phi_i(\mathbf{r}') \rangle}{\partial \omega} \right|_{\omega = \varepsilon_i} \right]^{-1}. \tag{2.55}$$

With this we have given the main points of the G_0W_0 method employed within this thesis. A detailed account of its implementation can be found in [32].

Starting from ground-state calculations that utilize PBE and PBE0′ exchange-correlation functionals we use G_0W_0 for the determination of band structures of the studied materials. Additionally, the obtained quasi-particle energies $\mathcal{E}_i^{qp}$ serve as an input for the following Bethe-Salpeter calculations.

2.3 Two-particle excitations

2.3.1 Bethe-Salpeter equation

We now turn our attention to neutral excitations - the electron-hole pairs arising in optical absorption experiments. A description using single-particle Green functions would not be sufficient here because it would disregard interactions between the involved particles like the electron-hole attraction. To account for these effects we need to examine the two-particle Green function G_2 leading to the Bethe-Salpeter equation (BSE).

For its derivation it is convenient to use the two-particle correlation function L instead of G_2. It is defined such that the motion of two independent particles is excluded from the two-particle Green function by subtracting the product GG from G_2:

$$L(1, \mathbf{r}'t; 2, \mathbf{r}t^+) = -G_2(1, \mathbf{r}'t; 2, \mathbf{r}t^+) + G(1, 2)\, G(\mathbf{r}'t, \mathbf{r}t^+). \qquad (2.56)$$

This definition coincides with the expression obtained by the variation of the single-particle Green function with respect to the non-local external potential in (2.21):

$$
\begin{aligned}
L(1, \mathbf{r}'t; 2, \mathbf{r}t^+) &= \frac{\delta G(1, 2)}{\delta U_{ext}(\mathbf{r}, \mathbf{r}', t)} \\
&= -\int \mathrm{d}(3, 4)\, G(1, 3)\, \frac{\delta G^{-1}(3, 4)}{\delta U_{ext}(\mathbf{r}, \mathbf{r}', t)}\, G(4, 2).
\end{aligned}
\qquad (2.57)
$$

In the second step we have used the functional derivative identity (2.28).

$G^{-1}(3, 4)$ can be rewritten by means of the Dyson equation in the following way. Taking into account the non-local external potential $U_{ext}(\mathbf{r}, \mathbf{r}', t)$ the Dyson equation (2.29) is now defined as:

$$\left[i\frac{\partial}{\partial t_1} - \hat{h}(1) - v_H(1)\right] G(1, 2) - \int \mathrm{d}(3)\, [U_{ext}(1, 3) + \Sigma(1, 3)]\, G(3, 2) = \delta(1, 2).$$
$$(2.58)$$

Multiplying it by $G^{-1}(2, 4)$ from the right and integrating over the variable (2) we get:

$$\left[i\frac{\partial}{\partial t_1} - \hat{h}(1) - v_H(1)\right] \delta(1, 2) - U_{ext}(1, 2) - \Sigma(1, 2) = G^{-1}(1, 2). \qquad (2.59)$$

Substituting $G^{-1}(3, 4)$ in Eq. (2.57) by means of the above expression we obtain:

$$L(1, \mathbf{r}'t; 2, \mathbf{r}t^+) =$$

$$= -\int \mathrm{d}(3, 4)\, G(1, 3)\, \frac{\delta\left\{\left[i\frac{\partial}{\partial t_3} - \hat{h}(3) - v_H(3)\right]\delta(3, 4) - U_{ext}(3, 4) - \Sigma(3, 4)\right\}}{\delta U_{ext}(\mathbf{r}, \mathbf{r}', t)} G(4, 2)$$

$$= \int \mathrm{d}(3, 4)\, G(1, 3) \left[\delta(\mathbf{r}, \mathbf{r}_3)\, \delta(\mathbf{r}', \mathbf{r}_4)\, \delta(t, t_3)\, \delta(t_3, t_4) + \frac{\delta\left[v_H(3)\, \delta(3, 4) + \Sigma(3, 4)\right]}{\delta U_{ext}(\mathbf{r}, \mathbf{r}', t)}\right] G(4, 2)$$

$$= G(1, \mathbf{r}t) \, G(\mathbf{r}'t, 2) + \int \mathrm{d}(3, 4) \, G(1, 3) \, \frac{\delta \left[v_H(3) \, \delta(3, 4) + \Sigma(3, 4) \right]}{\delta U_{ext}(\mathbf{r}, \mathbf{r}', t)} \, G(4, 2). \qquad (2.60)$$

By virtue of the the chain rule for functional derivatives we can write

$$\frac{\delta \left[v_H(3) \, \delta(3, 4) + \Sigma(3, 4) \right]}{\delta U_{ext}(\mathbf{r}, \mathbf{r}', t)}$$
$$= \int \mathrm{d}(5, 6) \, \frac{\delta \left[v_H(3) \, \delta(3, 4) + \Sigma(3, 4) \right]}{\delta G(5, 6)} \, \frac{\delta G(6, 5)}{\delta U_{ext}(\mathbf{r}, \mathbf{r}', t)}, \qquad (2.61)$$

where the second functional derivative expresses the two-particle correlation function $L(6, \mathbf{r}'t; 5, \mathbf{r}t^+)$. Introducing the effective two-particle interaction kernel Ξ:

$$\Xi(3, 5, 4, 6) = \frac{\delta \left[v_H(3) \, \delta(3, 4) + \Sigma(3, 4) \right]}{\delta G(5, 6)}, \qquad (2.62)$$

we can write:

$$L(1, \mathbf{r}'t; 2, \mathbf{r}t^+) = G(1, \mathbf{r}t)G(\mathbf{r}'t, 2) +$$
$$+ \int \mathrm{d}(3, 4, 5, 6) \, G(1, 3) \, G(4, 2) \, \Xi(3, 5, 4, 6) \, L(6, \mathbf{r}'t; 5, \mathbf{r}t^+). \qquad (2.63)$$

It is possible to generalize the above equation so that arbitrary time values can be substituted for t and t^+ [22]. Taking this into account and introducing the correlation function for two independent particles as

$$L_0(1, 1'; 2, 2') = G(1, 2') \, G(1', 2), \qquad (2.64)$$

we obtain the Bethe-Salpeter equation for the correlation function:

$$L(1, 1'; 2, 2') = L_0(1, 1'; 2, 2') + \int \mathrm{d}(3, 4, 5, 6) \, L_0(1, 4; 2, 3) \, \Xi(3, 5, 4, 6) \, L(6, 1'; 5, 2'). \qquad (2.65)$$

The structure of the equation is clearly comparable to that of the Dyson equation (2.34). The kernel Ξ relates the independent particle propagation L_0 to the correlation function L analogous to the self-energy Σ that links G_0 to G.

In practice, the exact form of the kernel Ξ is unknown. We want to review typical approximations in the next section.

2.3.2 Approximations for the effective interaction kernel Ξ

We can simplify the interaction kernel Ξ due to the fact that the derivative of the Hartree term can be straightforwardly evaluated:

$$\Xi(3, 5, 4, 6) = -i \int \mathrm{d}(2) \, v(3, 2) \, \frac{\delta G(2, 2^+)}{\delta G(5, 6)} \, \delta(3, 4) + \frac{\delta \Sigma(3, 4)}{\delta G(5, 6)}$$
$$= -i \, v(3, 6) \, \delta(5, 6) \, \delta(3, 4) + \frac{\delta \Sigma(3, 4)}{\delta G(5, 6)}. \qquad (2.66)$$

The form of Ξ already suggests the simplest approximation – neglecting the self-energy derivative so that only the bare Coulomb potential remains:

$$\Xi_H(3,5,4,6) = -i\,\delta(5,6)\,\delta(3,4)\,v(3,6). \qquad (2.67)$$

This is called the time-dependent Hartree approximation or Random-Phase Approximation (RPA), and it treats the motion of particles as that of free particles in an effective potential.

To account for interaction effects which are responsible for the formation of bound electron-hole states, the second term in Eq. (2.66) needs to be taken into consideration. The obvious approximation for the self-energy is the already discussed GW approximation: $\Sigma = iGW$. Then the evaluation of the second term Eq. (2.66) yields:

$$\frac{\delta\Sigma(3,4)}{\delta G(5,6)} = i\,\delta(3,5)\,\delta(4,6)\,W(3,4) + i\,G(3,4)\,\frac{\delta W(3,4)}{\delta G(5,6)}. \qquad (2.68)$$

The first term expresses the attractive electron-hole interaction that is proportional to the screened Coulomb interaction. The second term which describes the variation of the screening due to the excitation is considered to be small in comparison to the first term and is generally neglected. Thus, we arrive at the screened-interaction approximation which shall be employed in our calculations:

$$\Xi_{SI}(3,5,4,6) = -i\,\delta(5,6)\,\delta(3,4)\,v(3,6) + i\,\delta(3,5)\,\delta(4,6)\,W(3,4). \qquad (2.69)$$

In the following sections we want to depict a scheme for the solution of BSE within the screened-interaction approximation focusing especially on the connection of the BSE framework to quantities measurable by optical-absorption experiments.

2.3.3 Optical response from BSE

Before we outline a procedure leading to a solution of the Bethe-Salpeter equation let us clarify the exact relation between BSE and experimental quantities. In optical-absorption experiments we are interested in the average response of a macroscopic system to an optical perturbation. The measured absorption spectrum is given by the imaginary part of the macroscopic dielectric function ϵ_M. We have already introduced the microscopic dielectric function ϵ. It is possible to link it to ϵ_M on one hand and to the correlation function L on the other, so we want to discuss ϵ more carefully.

The application of an external perturbation U_{ext} on a system induces a screening potential V_{ind}, so that the total potential V acting on the system is given by:

$$V_{tot}(1) = U_{ext}(1) + V_{ind}(1). \qquad (2.70)$$

The microscopic dielectric function describes the response of the system in linear order, i.e., the change of the total potential given the perturbation:

$$V(1) = \int d(2)\,\epsilon^{-1}(1,2)\,U_{ext}(2). \qquad (2.71)$$

Using the definition (2.41) we can link the inverse dielectric function to the irreducible polarizability, which describes the response of the density to the variation of the perturbation:

$$
\begin{aligned}
\epsilon^{-1}(1,2) &= \frac{\delta V(1)}{\delta U_{ext}(2)} = \delta(1,2) - \int d(3)\, v(1,3)\, \frac{\delta\rho(1)}{\delta U_{ext}(2)} \\
&= \delta(1,2) - \int d(3)\, v(1,3)\, \chi(3,2).
\end{aligned}
\tag{2.72}
$$

Analogously a relation between the dielectric function and the reducible (complete) polarization can be derived, so we can write in matrix notation:

$$
\epsilon^{-1} = 1 + v\,\chi,
\tag{2.73}
$$

$$
\epsilon = 1 - v\,\tilde{\chi},
\tag{2.74}
$$

$$
\chi = \tilde{\chi} + \tilde{\chi}\,v\,\chi.
\tag{2.75}
$$

The last equation is a Dyson equation for the polarization χ and was obtained by combining the previous two. Its first term describes the polarization arising directly from the perturbation whereas the second term gives the polarization due to the field V_{ind} induced by the perturbation.

Using the definition of the polarization χ (Eq. (2.41)) we get a connection to the correlation function:

$$
\begin{aligned}
\tilde{\chi}(1,2) &= -i\,\frac{\delta G(1,1^+)}{\delta U_{ext}(2)} = -i\,[G_2(1,2;1^+,2^+) - G(1,1^+)\,G(2,2^+)] \\
&= -i\,L(1,2;1^+,2^+).
\end{aligned}
\tag{2.76}
$$

So we can obtain the dielectric function ϵ from the two-particle correlation function L by means of the polarizability.

On the other hand, Adler [33] and Wiser [34] showed that the macroscopic dielectric function is related to its microscopic equivalent by:

$$
\epsilon_M(\omega) = \frac{1}{\epsilon^{-1}_{\mathbf{G}=0,\mathbf{G}'=0}(\mathbf{q},\omega)},
\tag{2.77}
$$

where $\epsilon_{\mathbf{G},\mathbf{G}'}(\mathbf{q},\omega) = \epsilon(\mathbf{q}+\mathbf{G},\mathbf{q}+\mathbf{G}',\omega)$ is the Fourier transform of the dielectric function $\epsilon(\mathbf{r},\mathbf{r}',t-t')$ to the reciprocal space and frequency domain. $\mathbf{q}$ denotes a vector belonging to the first Brillouin zone, and $\mathbf{G}$ is a reciprocal lattice vector. Thus, the macroscopic dielectric function is given by the $\mathbf{G}=0, \mathbf{G}'=0$ component of the *inverse* dielectric function which means that all components of $\epsilon(\mathbf{q},\omega)$ contribute to $\epsilon_M(\omega)$. The physical meaning behind that is the following: We consider a perturbing external field that varies slowly over the size of the unit cell. But due to the inhomogeneity of the system (the dielectric function depends on the positions $\mathbf{r}$ and $\mathbf{r}'$ and not on the distance $\mathbf{r}-\mathbf{r}'$) the induced screening fields and hence the total fields vary on the atomic scale. This behavior is referred to as local-field effects.

There is another issue we have to take into account. We are interested in optical perturbations – their wavelengths being large compared to the unit cell size, which corresponds to small $\mathbf{q}$ vectors. Thus, the correct treatment of optical perturbations means taking the limit of vanishing $\mathbf{q}$. In this case a divergent term stemming from the Coulomb interaction arises in the Dyson equation for the polarizability (2.75). Ambegaokar and Kohn [35] managed to avoid the problem by defining a modified polarizability $\bar{\chi}$ that excludes terms with divergent long-range part of the Coulomb potential:

$$\bar{\chi} = \tilde{\chi} + \tilde{\chi}\,\bar{v}\,\bar{\chi}, \tag{2.78}$$

with $\bar{v}$ given by

$$\bar{v}_{\mathbf{G}}(\mathbf{q}) = \begin{cases} 0, & \mathbf{G} = 0 \\ v_{\mathbf{G}}(\mathbf{q}), & \mathbf{G} \neq 0. \end{cases} \tag{2.79}$$

Then the expression for the macroscopic dielectric function is modified to be:

$$\epsilon_M(\mathbf{q}, \omega) = 1 - \lim_{\mathbf{q} \to 0} v(\mathbf{q})\,\bar{\chi}_{\mathbf{G}=0,\mathbf{G}'=0}(\mathbf{q}, \omega), \tag{2.80}$$

where the polarization is obtained from the BSE calculation by means of Eq. (2.76).

2.3.4 Reformulation of BSE as an eigenvalue problem

Now we briefly outline the procedure leading to the solution of BSE, which is extensively explained in [36, 37]. The strategy consists of transforming the integral equation (2.65) into an eigenvalue problem by expanding the electron-hole correlation function in terms of quasi-particle wave functions.

First two simplifications are applied. Within the scope of optical excitations we want to discuss the simultaneous propagation and interaction of the considered particles, the electron and the hole, which means setting $t_1 = t_{1'}$ and $t_2 = t_{2'}$ in the correlation function $L(1, 1'; 2, 2')$. Due to the translational invariance in time L depends on the time difference $t_1 - t_2$ which is transformed to frequency space ω where the discussion shall be conducted. Further, the approximation of a static screened Coulomb interaction W is made following the argumentation by Bechstedt *et al.* [38] that the dynamical effects of the screening and one-particle Green function cancel each other. The correlation function is now $L = L(\mathbf{r}_1, \mathbf{r}_1', \mathbf{r}_2, \mathbf{r}_2', \omega)$, and we can symbolically write the BSE as:

$$L(\omega) = L_0(\omega) + L(\omega)\,\Xi\,L(\omega). \tag{2.81}$$

As we have seen in previous sections, the excitations of single particles can be described by quasi-particle wave functions and energies. It seems obvious to use these quantities as we consider the propagation and interaction of two particles, *i.e.*, to expand the correlation function $L = L(\mathbf{r}_1, \mathbf{r}_1', \mathbf{r}_2, \mathbf{r}_2', \omega)$ in a basis of quasi-particle wave functions. Following the G_0W_0 discussion in Section 2.2.4, the quasi-particle

wave functions are approximated by the Kohn-Sham ones:

$$L(\mathbf{r}_1, \mathbf{r}_1', \mathbf{r}_2, \mathbf{r}_2', \omega) = \sum_{i_1 i_2 i_3 i_4} \phi_{i_1}^*(\mathbf{r}_1)\, \phi_{i_2}(\mathbf{r}_1')\, \phi_{i_3}(\mathbf{r}_2)\, \phi_{i_4}^*(\mathbf{r}_2')\, L_{(i_1 i_2),(i_3 i_4)}, \qquad (2.82)$$

with the expansion coefficients given by:

$$L_{(i_1 i_2),(i_3 i_4)} = \int \mathrm{d}\mathbf{r}_1 \mathrm{d}\mathbf{r}_1' \mathrm{d}\mathbf{r}_2 \mathrm{d}\mathbf{r}_2'\, \phi_{i_1}^*(\mathbf{r}_1)\, \phi_{i_2}(\mathbf{r}_1')\, \phi_{i_3}(\mathbf{r}_2)\, \phi_{i_4}^*(\mathbf{r}_2')\, L(\mathbf{r}_1, \mathbf{r}_1', \mathbf{r}_2, \mathbf{r}_2', \omega). \quad (2.83)$$

Since L_0 is a product of two one-particle Green functions we can readily express it by employing the $G_0 W_0$ approximation for the one-particle Green function (Eq. (2.50)):

$$G(\mathbf{r}, \mathbf{r}'; \omega) = \sum_{n\mathbf{k}} \frac{\phi_{n\mathbf{k}}(\mathbf{r})\, \phi_{n\mathbf{k}}^*(\mathbf{r}')}{\omega - \mathcal{E}_{n\mathbf{k}} - i\eta\, \mathrm{sgn}(\mu - \mathcal{E}_{n\mathbf{k}})}. \qquad (2.84)$$

In the denominator we can use the quasi-particle energies $\mathcal{E}_{n\mathbf{k}}$ obtained from the preceding $G_0 W_0$ calculation. The Fourier transformation of L_0 taking into account the above equation yields

$$L_0(\mathbf{r}_1, \mathbf{r}_1', \mathbf{r}_2, \mathbf{r}_2', \omega) = i \sum_{i_1 i_2 i_3 i_4} \frac{\phi_{i_1}^*(\mathbf{r}_1)\, \phi_{i_2}(\mathbf{r}_1')\, \phi_{i_3}(\mathbf{r}_2)\, \phi_{i_4}^*(\mathbf{r}_2')}{\mathcal{E}_{i_2}^{qp} - \mathcal{E}_{i_1}^{qp} - \omega - i\eta}\, (f_{i_2} - f_{i_1})\, \delta_{i_1,i_3}\, \delta_{i_2,i_4}, \tag{2.85}$$

with f_i denoting the Fermi-Dirac distribution functions - the occupation numbers of the orbitals. Seeing that L_0 can be expanded similarly to L (Eq. (2.82)), we can identify the expansion coefficients in the above equation as

$$L_{(i_1 i_2),(i_3 i_4)}^0 = -i\, \frac{(f_{i_2} - f_{i_1})\, \delta_{i_1,i_3}\, \delta_{i_2,i_4}}{\mathcal{E}_{i_2}^{qp} - \mathcal{E}_{i_1}^{qp} - \omega - i\eta}. \qquad (2.86)$$

It is then possible to reformulate Eq. (2.81) as

$$L_{(i_1 i_2),(i_3 i_4)}(\omega) = i\, [H^{e-h} - \omega]_{(i_1 i_2),(i_3 i_4)}^{-1}\, (f_{i_4} - f_{i_3}), \qquad (2.87)$$

with the electron-hole Hamiltonian

$$H_{(j_1 j_2),(j_3 j_4)}^{e-h} = (E_{j_2} - E_{j_1})\, \delta_{i_1,i_3}\, \delta_{i_2,i_4} - i\, (f_{j_2} - f_{j_1})\, \Xi_{(j_1 j_2),(j_3 j_4)}. \qquad (2.88)$$

It is thus necessary to invert the matrix $H^{e-h} - \omega$ to obtain the expansion coefficients for the correlation function. In general the structure of the electron-hole Hamiltonian is complicated due to the various orbital-index combinations. However, the Hamiltonian takes on a more simple form for systems with a band gap where we have occupied valence states v and unoccupied conduction states c. In that case the factor denoting the difference of occupation numbers $f_{j_2} - f_{j_1}$ is zero for $v - v$ and $c - c$ combinations. In detail, the analysis of H^{e-h} is given in [36], here, we present the remaining Hamiltonian which can be divided in four blocks:

$$H^{eff} = \begin{pmatrix} H_{(v c \mathbf{k}),(v' c' \mathbf{k}')}^{res} & H_{(v c \mathbf{k}),(c' v' \mathbf{k}')}^{coupling} \\ -[H_{(v c \mathbf{k}),(c' v' \mathbf{k}')}^{coupling}]^* & H_{(v c \mathbf{k}),(v' c' \mathbf{k}')}^{antires} \end{pmatrix}, \qquad (2.89)$$

31

with

$$H^{res}_{(vc\mathbf{k}),(v'c'\mathbf{k'})} = (\mathcal{E}^{qp}_{c\mathbf{k}} - \mathcal{E}^{qp}_{v\mathbf{k}})\,\delta_{vv'}\,\delta_{cc'}\,\delta_{\mathbf{k}\mathbf{k'}} + i\,\Xi_{vc\mathbf{k},v'c'\mathbf{k'}}, \tag{2.90}$$

$$H^{coupling}_{(vc\mathbf{k}),(c'v'\mathbf{k'})} = i\,\Xi_{vc\mathbf{k},c'v'\mathbf{k'}}, \tag{2.91}$$

$$H^{antires}_{(vc\mathbf{k}),(v'c'\mathbf{k'})} = -[H^{res}_{(vc\mathbf{k}),(v'c'\mathbf{k'})}]^*. \tag{2.92}$$

Hereby, we express the orbital index i through the corresponding Bloch vector $\mathbf{k}$ and the band index v for valence or c for conduction states.

Thus, the diagonal matrices contain quasi-particle energy differences and the electron-hole interaction kernel Ξ, whereas only the kernel contributes to the off-diagonal coupling matrices. Consequently, for systems with a band gap larger then the electron-hole interaction strength, the coupling matrices would be small compared to the diagonal ones. In that case the Tamm-Dancoff approximation [21] to neglect the coupling matrices is applied. The approximation is justified for most semiconductors and is employed in our calculations.

From the diagonal matrices that remain, the resonant part contributes to positive frequencies and the antiresonant part contributes to negative ones. We have now reduced the problem of solving the Bethe-Salpeter equation to diagonalizing the Hermitian resonant contribution $H^{res}_{(vc\mathbf{k}),(v'c'\mathbf{k})}$ expressed by the following eigenvalue equation:

$$\sum_{v'c'\mathbf{k'}} H^{res}_{vc\mathbf{k},v'c'\mathbf{k'}}\,A^{\lambda}_{v'c'\mathbf{k'}} = E^{\lambda}\,A^{\lambda}_{vc\mathbf{k}}. \tag{2.93}$$

2.3.5 The effective electron-hole Hamiltonian

Let us summarize the terms comprising the Hamiltonian. The large diagonal term consists of the quasi-particle energy differences, two other terms – called the direct and the exchange terms – stem from the electron-hole interaction kernel (2.69). Using the relation (2.82) the kernel is reformulated in the quasi-particle basis, with the expansion coefficients calculated by means of (2.83). Thus, the terms are explicitly given by:

$$H^{diag}_{vc\mathbf{k},v'c'\mathbf{k'}} = (\mathcal{E}^{qp}_{c\mathbf{k}} - \mathcal{E}^{qp}_{v\mathbf{k}})\,\delta_{vv'}\,\delta_{cc'}\,\delta_{\mathbf{k}\mathbf{k'}}, \tag{2.94}$$

$$H^{dir}_{vc\mathbf{k},v'c'\mathbf{k'}} = -\int \mathrm{d}\mathbf{r}\mathrm{d}\mathbf{r'}\,\phi_{v\mathbf{k}}(\mathbf{r})\,\phi^*_{c\mathbf{k}}(\mathbf{r'})\,W(\mathbf{r},\mathbf{r'})\,\phi^*_{v'\mathbf{k'}}(\mathbf{r})\,\phi_{c'\mathbf{k'}}(\mathbf{r'}), \tag{2.95}$$

$$H^{x}_{vc\mathbf{k},v'c'\mathbf{k'}} = \int \mathrm{d}\mathbf{r}\mathrm{d}\mathbf{r'}\,\phi_{v\mathbf{k}}(\mathbf{r})\,\phi^*_{c\mathbf{k}}(\mathbf{r})\,\bar{v}(\mathbf{r},\mathbf{r'})\,\phi^*_{v'\mathbf{k'}}(\mathbf{r'})\,\phi_{c'\mathbf{k'}}(\mathbf{r'}). \tag{2.96}$$

The direct term H^{dir} contains the screened Coulomb interaction. Its attractive nature is responsible for the formation of bound electron-hole pairs. The exchange term contains the bare Coulomb interaction without the long-range part in accordance with the discussion in Section 2.3.3.

Then, the Hamiltonian can be written as

$$H^{res} = H^{diag} + \gamma_{dir} H^{dir} + \gamma_x H^x \tag{2.97}$$

with the factors γ_{dir} and γ_x letting us distinguish between different levels of approximation and spin channels. If both factors are set to zero we arrive at the non-interacting independent particle approximation. By taking into account the exchange term ($\gamma_{dir} = 0$, $\gamma_x = 1$) we include the local-field effects. The exchange term is also important in the context of the spin structure of the Hamiltonian. For systems with weak spin-orbit coupling compared to the electron-hole interaction the single-particle states can be classified as spin up or spin down states [36, 22], so that four subspaces emerge: $|v_\uparrow c_\uparrow \mathbf{k}\rangle$, $|v_\downarrow c_\downarrow \mathbf{k},\rangle$ $|v_\uparrow c_\downarrow \mathbf{k}\rangle$, $|v_\downarrow c_\uparrow \mathbf{k}\rangle$. When the matrix elements of the Hamiltonian between these subspaces are evaluated, one can see that the Hamiltonian decouples into a spin-singlet and spin-triplet type of solutions. The spin-singlet type corresponds to the subspace

$$\left\{ \frac{1}{\sqrt{2}} (|v_\uparrow c_\uparrow \mathbf{k}\rangle + |v_\downarrow c_\downarrow \mathbf{k}\rangle) \right\}, \tag{2.98}$$

with the Hamiltonian

$$H^{singlet} = H^{diag} + H^{dir} + 2H^x. \tag{2.99}$$

The triplet configuration is formed by the subspaces

$$\left\{ |v_\uparrow c_\downarrow \mathbf{k}\rangle, \quad |v_\downarrow c_\uparrow \mathbf{k}\rangle, \quad \frac{1}{\sqrt{2}} (|v_\uparrow c_\uparrow \mathbf{k}\rangle - |v_\downarrow c_\downarrow \mathbf{k}\rangle) \right\}, \tag{2.100}$$

corresponding to the Hamiltonian

$$H^{triplet} = H^{diag} + H^{dir}. \tag{2.101}$$

So the exchange term controls the splitting between singlet and triplet type of solutions.

We apply the different levels of approximation to our calculations and compare the results in Chapter 4.

2.3.6 Macroscopic dielectric function

Knowing the eigenvalues E^λ and eigenvectors $A_{vc\mathbf{k}}^\lambda$ of the Hamiltonian H^{e-h} the correlation function (2.87) can be reformulated by means of the spectral theorem as

$$L_{vc\mathbf{k},v'c'\mathbf{k}'}(\omega) = -i \sum_\lambda \frac{A_{vc\mathbf{k}}^\lambda [A_{v'c'\mathbf{k}'}^\lambda]^*}{E^\lambda - \omega}. \tag{2.102}$$

In the next steps, the real-space representation of L (Eq. (2.82)) is related to the polarization $\bar{P}$ by means of Eq. (2.76), the polarization is transformed to reciprocal

space, and its $\mathbf{G} = 0, \mathbf{G}' = 0$ component is used in the calculation of the macroscopic dielectric function (Eq. (2.80)). After taking the limit $\mathbf{q} \to 0$ one eventually arrives at the following expression for the imaginary part of the macroscopic dielectric function:

$$\mathrm{Im}\,\epsilon_M(\omega) = \frac{8\pi^2}{\Omega} \sum_\lambda \left| \sum_{vc\mathbf{k}} A_{vc\mathbf{k}}^\lambda \frac{\langle v\mathbf{k}|\mathbf{p}|c\mathbf{k}\rangle^{DFT}}{\mathcal{E}_{c\mathbf{k}}^{qp} - \mathcal{E}_{v\mathbf{k}}^{qp}} \right|^2 \delta(E^\lambda - \omega). \qquad (2.103)$$

where $\mathbf{p}$ denotes the momentum operator and Ω the crystal volume. The detailed discussion of the derivation can be found in [39].

Chapter 3

The full potential (L)APW+lo method

3.1 Generalized eigenvalue problem

In this chapter we want to clarify how to solve the Kohn-Sham equations numerically. There exists a variety of methods to accomplish this task: Functions can be sampled on a real-space grid or expanded in reciprocal space, one can take all electrons into account or employ pseudo-potential approximations. The approach implemented within **exciting**, an all electron full potential (L)APW+lo method, is among the most accurate ones. As a basis-set based approach it can be generally outlined as follows.

The Kohn-Sham wave functions ϕ_i are expanded in terms of a basis set $\{\varphi_j(\mathbf{r})\}$ most fitting to the problem at hand:

$$\phi_i(\mathbf{r}) = \sum_j C_{ji}\, \varphi_j(\mathbf{r}), \tag{3.1}$$

with expansion coefficients C_{ji}. Inserting this expansion into the Kohn-Sham equation (1.24), multiplying the result with $\varphi_l^*(\mathbf{r})$ from the left and integrating over $\mathbf{r}$ gives:

$$\sum_j H_{lj}\, C_{ji} = \varepsilon_i \sum_j S_{lj}\, C_{ji}, \tag{3.2}$$

i.e. the Kohn-Sham equations are transformed into a generalized eigenvalue problem. By H_{lj} we denote the matrix elements of the single-particle Kohn-Sham Hamiltonian $h(\mathbf{r})$ consisting of the kinetic energy operator and the Kohn-Sham effective potential:

$$H_{lj} = \int d\mathbf{r}\, \varphi_l^*(\mathbf{r})\, \hat{h}(\mathbf{r})\, \varphi_j(\mathbf{r}). \tag{3.3}$$

S_{lj} is the overlap matrix arising if the basis set is nonorthogonal:

$$S_{lj} = \int d\mathbf{r}\, \varphi_l^*(\mathbf{r})\, \varphi_j(\mathbf{r}). \tag{3.4}$$

The choice of a basis set is an important one in regards to computational efficiency. Since we consider crystals, *i.e.* systems with periodic boundary conditions, plane waves seem a natural choice. They are orthogonal and analytically easy to handle. However, in the region of the nuclei electrons are still strongly bound and are best represented by wave functions of rapidly varying nature similar to the atomic ones. Consequently, an exceedingly large number of plane waves would be necessary to describe electrons in the vicinity of the nuclei. A pure plane wave approach is therefore computationally impractical. It was Slater [40] in 1937 who first suggested to augment plane waves by atomic-like functions in the regions of the nuclei establishing the APW (augmented plane wave) approach. The variations of this idea are nowadays widely used for density-functional-theory problems.

3.2 APW basis

The main idea of APW and related methods is to divide the crystal in two regions: the non-overlapping *muffin-tin spheres* (MT) centered around the atoms and the *interstitial space* (I) in between. Atomic-like functions are employed to describe the oscillating nature of the wave functions inside the muffin-tin spheres. In the interstitial region plane waves are most apt to describe the slow-varying wave functions. The APW basis set is then written in the following way:
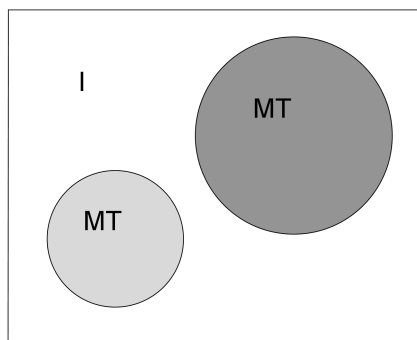
Figure 3.1: Division of the unit cell in the interstitial (I) and and muffin-tin (MT) region

$$\varphi_{\mathbf{k}}^{APW}(\mathbf{r}, \epsilon_l) = \begin{cases} \frac{1}{\sqrt{\Omega}} e^{i(\mathbf{k}+\mathbf{G})\cdot\mathbf{r}} & \mathbf{r} \in \mathrm{I} \\ \sum_{\alpha,lm} A_{lm}^{\alpha}(\mathbf{k}+\mathbf{G}) \, u_l(r_\alpha, \epsilon_l) \, Y_{lm}(\hat{\mathbf{r}}_\alpha) & \mathbf{r} \in \mathrm{MT} \end{cases}, \qquad (3.5)$$

where $\mathbf{k}$ denotes a vector within the first Brillouin zone and $\mathbf{G}$ a reciprocal lattice vector. In the muffin-tin region the wave functions are built from radial functions $u_l(r_\alpha, \epsilon_l)$ times spherical harmonics $Y_{lm}(\mathbf{r}_\alpha)$. $\mathbf{r}_\alpha$ denotes hereby a vector $\mathbf{r} - \mathbf{R}_\alpha$ with $\mathbf{R}_\alpha$ as the center of a muffin-tin sphere around the atom α. The radial functions $u_l(r_\alpha, \epsilon_l)$ are determined by solving the radial Schrödinger equation

$$\left\{ -\frac{1}{2} \frac{\partial^2}{\partial r_\alpha^2} + \frac{l(l+1)}{2r_\alpha^2} + v_{KS}(r_\alpha) - \epsilon_l \right\} r_\alpha u_l(r_\alpha, \epsilon_l) = 0, \qquad (3.6)$$

with the spherical component of the Kohn-Sham potential $v_{KS}(r_\alpha)$. The coefficients $A_{lm,\mathbf{k}+\mathbf{G}}$ are constructed in such a way that each muffin-tin function matches a plane wave at the muffin-tin boundary. Thus the plane waves are augmented by the muffin-tin functions.

The Kohn-Sham potential can be handled in different ways. To reduce the computational cost it is common to apply shape approximations for the potential, *e.g.* the exact potential is considered only in the muffin-tin spheres, and in the interstitial it is set to a constant. Contrary to that approach the full potential (FP) is taken into account here providing the best possible accuracy for the APW-related methods. The potential is expanded in a similar way to the wave functions:

$$
v_{KS}(\mathbf{r}) = \begin{cases} \sum\limits_{\mathbf{G}} V_{\mathbf{G}}\, e^{i\mathbf{G}\,\mathbf{r}} & \mathbf{r} \in \mathrm{I} \\[2mm] \sum\limits_{lm} V_{lm}(r)\, Y_{lm}(\hat{\mathbf{r}}) & \mathbf{r} \in \mathrm{MT} \end{cases} . \tag{3.7}
$$

The pure APW approach has a significant disadvantage. By construction each APW function depends on the energies ϵ_l through the radial functions $u_l(r_\alpha, \epsilon_l)$. However these are the energies we want to determine by solving the generalized eigenvalue problem, they are not known beforehand. The problem becomes nonlinear in energy. To solve it one would have to perform multiple consecutive rounds of diagonalization: Starting with a trial energy for ϵ_l the APW basis is built and Eq. (3.2) is diagonalized. If the obtained eigenvalues differ from ϵ_l new trial energies are taken and the procedure is repeated until both match. This is clearly an inefficient approach. It is improved by the method called linearized APW (LAPW) developed by Anderson in 1975.

3.3 LAPW basis

In LAPW, the energies ϵ_l enter the calculation as parameters used to construct the basis that don't have to be equal to the Kohn-Sham band energies. This is achieved by expanding the radial functions in a Taylor series around ϵ_l up to the linear term:

$$
u_l(r_\alpha, \epsilon) = u_l(r_\alpha, \epsilon_l) + (\epsilon - \epsilon_l)\, \dot{u}_l(r_\alpha, \epsilon_l) + \mathcal{O}[(\epsilon - \epsilon_l)^2]. \tag{3.8}
$$

$\dot{u}_l(r_\alpha, \epsilon_l)$ denotes the derivative $\partial u_l(r_\alpha, \epsilon)/\partial\epsilon$ calculated at $\epsilon = \epsilon_l$. The error in the Kohn-Sham wave functions is therefore quadratic in the deviation of the true eigenvalue from the chosen linearization energy ϵ_l. This amounts to an error of the fourth order in the eigenvalues themselves. So we see that the termination of the expansion after the linear term still allows us to cover a broad energy region around the linearization energy because of the high order of the linearization error. To minimize it ϵ_l are typically chosen to lie in the center of the corresponding l-like band.

Accounting for Eq. (3.8) the LAPW basis is now described by the following equations:

$$
\varphi_{\mathbf{k}}^{LAPW}(\mathbf{r}, \epsilon_l) = \begin{cases} \dfrac{1}{\sqrt{\Omega}} e^{i(\mathbf{k}+\mathbf{G})\cdot\mathbf{r}} & \mathbf{r} \in \mathrm{I} \\[2mm] \sum\limits_{\alpha, lm} \left[A_{lm}^\alpha(\mathbf{k}+\mathbf{G})\, u_l(r_\alpha, \epsilon_l) + B_{lm}^\alpha(\mathbf{k}+\mathbf{G})\, \dot{u}_l(r_\alpha, \epsilon_l) \right] Y_{lm}(\hat{\mathbf{r}}_\alpha) & \mathbf{r} \in \mathrm{MT} \end{cases} .
$$

$$\tag{3.9}$$

The new matching coefficients $B_{lm,\mathbf{k+G}}$ are determined by requiring that the first derivatives of the basis functions with respect to r are continuous at the muffin-tin boundary. The condition for $A_{lm,\mathbf{k+G}}$ stated above remains. $\dot{u}_l(r_\alpha,\epsilon_l)$ are calculated by integrating the Schrödinger-like equation obtained after taking the energy derivative of (3.6):

$$\left\{-\frac{1}{2}\frac{\partial^2}{\partial r_\alpha^2} + \frac{l(l+1)}{2r_\alpha^2} + v_{KS}(r_\alpha)\right\} r_\alpha\dot{u}_l(r_\alpha,\epsilon_l) = r_\alpha u_l(r_\alpha,\epsilon_l) + \epsilon_l r_\alpha\dot{u}_l(r_\alpha,\epsilon_l). \quad (3.10)$$

Furthermore an orthogonality condition is imposed on $u_l(r_\alpha,\epsilon_l)$ and $\dot{u}_l(r_\alpha,\epsilon_l)$.

LAPW manages to avoid the nonlinearity problem of APW by removing the band energy dependence from the basis and consequently making one diagonalization for a given Kohn-Sham potential sufficient. But this is done at a price of a larger basis size: the necessity to match the muffin-tin functions and plane waves up to the first derivative requires a higher plane wave cut-off for the same accuracy as in the APW method. It is possible to combine the advantages of both approaches in the APW+lo basis set suggested by Sjöstedt *et al.* [41].

3.4 APW+lo basis

The idea of APW+lo is to supplement the APW basis (3.5) with local orbitals (lo). For construction of the APW basis set fixed linearization energies ϵ_l are taken. To improve the variational freedom of the basis and avoid the problem of having to diagonalize the Hamiltonian several times as described in Section 3.2 local orbitals are added:

$$\varphi_{lm}^{\alpha,lo}(\mathbf{r}) = \begin{cases} 0 & \mathbf{r} \in \mathrm{I} \\ \left[A_{lm}^{\alpha,lo}\, u_l(r_\alpha,\epsilon_l) + B_{lm}^{\alpha,lo}\, \dot{u}_l(r_\alpha,\epsilon_l)\right] Y_{lm}(\hat{\mathbf{r}}_\alpha) & \mathbf{r} \in \mathrm{MT} \end{cases}. \quad (3.11)$$

The radial functions $u_l(r_\alpha,\epsilon_l)$ and its energy derivatives are evaluated at the energy ϵ_l of the corresponding APW orbital. The coefficients $A_{lm}^{\alpha,lo}$ and $B_{lm}^{\alpha,lo}$ are calculated by imposing the normalization condition upon the local orbital and by requiring that it vanishes at the muffin-tin boundary. So the basis size for APW+lo is comparable to that of APW. Throughout this work the APW+lo method is used.

3.5 Local orbitals for semi-core states

When describing different states of an atom participating in chemical bonding with neighboring atoms another issue arises. The electrons of the considered atom can be generally separated into two types. There are those strongly bound to the nucleus that behave essentially as if they were in a free atom. They are confined to the muffin-tin spheres and are not involved in chemical bonding. These are called *core* electrons. The second type are the *valence* electrons with an energy lying close to

the Fermi level. They leak out of muffin-tin spheres and bond with electrons of other atoms. The corresponding valence states are taken into account during the construction of the basis (3.9).

For some materials it is hard to draw a clear distinction between the two types. In particular there are certain states near the core region with a low principle quantum number n that are not wholly confined to the muffin-tin sphere, but have the same angular momentum l as some valence states with a higher n. Since these so-called *semi-core* states can not be accounted for by the same ϵ_l as the higher lying valence states, the question arises how to treat them. The problem is handled by introducing additional basis functions also called local orbitals [42]. As they are not the same type of local orbitals as defined in the previous section, we label these local orbitals by 'LO'. These are linear combinations of three radial functions: The LAPW functions $u_l(r_\alpha, \epsilon_l)$ and $\dot{u}_l(r_\alpha, \epsilon_l)$ and a new function $u_{l_{LO}}(r_\alpha, \epsilon_l^{LO})$ that is determined using the energy parameter $\epsilon_{l_{LO}}$ set to the energy of the semi-core state to be described. So the local orbital added to an atom α for a state with an angular momentum l has the following form:

$$\varphi_{lm}^{\alpha,LO}(\mathbf{r}) = \begin{cases} 0 & \mathbf{r} \in \mathrm{I} \\ \left[A_{lm}^{\alpha,LO} u_l(r_\alpha, \epsilon_l) \quad + B_{lm}^{\alpha,LO} \dot{u}_l(r_\alpha, \epsilon_l) \right. \\ \qquad \left. + C_{lm}^{\alpha,LO} u_l(r_\alpha, \epsilon_l^{LO}) \right] Y_{lm}(\hat{\mathbf{r}}_\alpha) & \mathbf{r} \in \mathrm{MT} \end{cases} . \quad (3.12)$$

The coefficients $A_{lm}^{\alpha,LO}$, $B_{lm}^{\alpha,LO}$ and $C_{lm}^{\alpha,LO}$ are chosen such that the local orbital is normalized and vanishes at the muffin-tin boundary in value and slope. The local orbital is completely confined to the sphere of atom α. It has zero value in the muffin-tin spheres of other atoms and in the interstitial.

Chapter 4

Results

We investigate bulk rutile and anatase TiO_2 by means of methodologies outlined in the preceding chapters. Hereby, the **exciting** code [2] is used for all computations. After a short review of the structure of both crystals we present results of ground-state calculations, the band structure and the optical spectra. As indicated in the first chapter, the Kohn-Sham ground-state calculations are carried out using two different types of exchange-correlation potentials: PBE and the hybrid PBE0′. In the subsequent G_0W_0 and BSE calculations we investigate whether the excited state properties are influenced by the choice of the exchange-correlation potential. We compare the calculated band gaps and optical absorption spectra to the available theoretical and experimental data.

4.1 Crystal structure

Rutile and anatase are the most common phases of TiO_2 to be found in nature. Both phases crystallize in a tetragonal structure (Fig.4.1). Rutile exhibits a simple tetragonal structure with the lattice parameters $a = b = 4.593$ Å and $c = 2.959$ Å [43] and belongs to the space group $P4_2/mnm$. Anatase is characterized by a body-centered tetragonal structure with lattice parameters $a = b = 3.73$ Å and $c = 9.37$ Å [44]. The spacial group of anatase is $I4_1/amd$. In rutile phase, TiO_2 contains 6 atoms per primitive unit cell, in the anatase phase there are 12 atoms in a conventional unit cell. In both phases, the titanium atom is surrounded by a distorted octahedron formed by six oxygen atoms. The TiO_6 octahedron shares two edges with its neighbours in rutile, while in anatase four edges are shared with the neighboring octahedra.
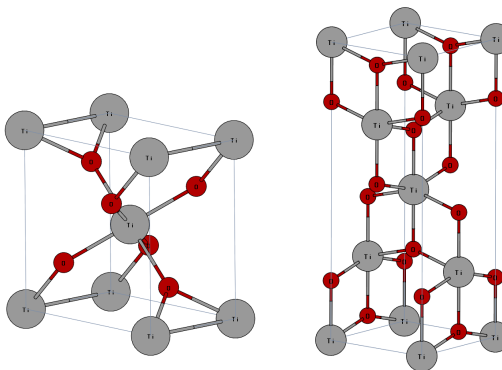
Figure 4.1: Unit cells of rutile (left) and anatase (right) TiO_2

4.2 Ground-state calculations

We proceed by first investigating the convergence of the PBE-based ground-state calculations with respect to numerical cut-off parameters. Thereupon a structure optimization of the unit cell is performed with the PBE functional. The obtained equilibrium structure is used for all subsequent calculations including the PBE0′-based ones. Let us discuss these steps in more detail.

4.2.1 Ground-state convergence tests

To investigate the convergence behavior of the PBE-based and following that, the PBE0′-based and G_0W_0 calculations, we monitor the band gap. The convergence tests are conducted with respect to the parameters crucial to the accuracy of the calculation – RGk_{max} and the $\mathbf{k}$-grid. The first parameter characterizes the quality of the basis set: It represents the product of the smallest muffin-tin radius R and the largest $\mathbf{k} + \mathbf{G}$ vector $Gk_{max} = |\mathbf{k} + \mathbf{G}|_{max}$ in the APW+lo basis functions (3.5) thus implicitly determining the number of basis functions. RGk_{max} captures the interplay between the muffin-tin radius and the number of plane waves: A small muffin-tin radius requires a large number of plane waves to describe the wave functions in the vicinity of the nucleus outside of the muffin-tin sphere, whereas a smaller number of plane waves suffices for a big muffin-tin radius.

Let us also remark upon the partitioning of the core and the valence region within the APW+(lo) method at this point. In oxygen, $1s$ electrons are treated as core and $2s\,2p$ electrons as valence electrons. In titanium $1s\,2s\,2p$ states are treated as the core and the $3s\,3p\,4s\,3d$ states as the valence region.

The $\mathbf{k}$-grid determines the number of Bloch vectors ($\mathbf{k}$-points) entering the calculation. In principle, an infinite number of $\mathbf{k}$-points is needed to describe every point in the first Brillouin zone. Evaluation of observables such as the total energy necessitates the calculation of integrals over all $\mathbf{k}$-points. Such calculations are very demanding, so in practice, the integration is approximated by a sum performed over a finite number of $\mathbf{k}$-points distributed on a mesh. Some of the $\mathbf{k}$-points are equivalent due to crystal-symmetry considerations, so the calculations can be performed with a reduced set of $\mathbf{k}$-points in the *irreducible* part of the Brillouin zone. Semiconductors generally require a small number of $\mathbf{k}$-points. The summation over the Brillouin zone is carried out utilizing the tetrahedron method.

The results of the convergence tests for the Kohn-Sham band gap are presented in Fig. 4.2 for rutile and anatase. In the case of the $\mathbf{k}$-grid only the number of $\mathbf{k}$-points in k_x direction is shown. We choose the ratio of the number of $\mathbf{k}$-points in each direction to approximately represent the the ratio of the reciprocal lattice parameters. Thus, the sampled $\mathbf{k}$-points are distributed in an approximately uniform way in the unit cell. Then, the mesh $n_{k_x} \times n_{k_y} \times n_{k_z}$ becomes $n_{k_x} \times n_{k_x} \times 1.5 \cdot n_{k_x}$ for rutile and $n_{k_x} \times n_{k_x} \times n_{k_x} \cdot 0.4$ for anatase.

Guided by the convergence tests we choose $RGk_{max} = 7$ for both crystals, which gives us an accuracy of 0.005 eV. With the muffin-tin radii of 2 Bohr for titanium and 1.45 Bohr for oxygen, the chosen RGk_{max} corresponds to 880 basis functions
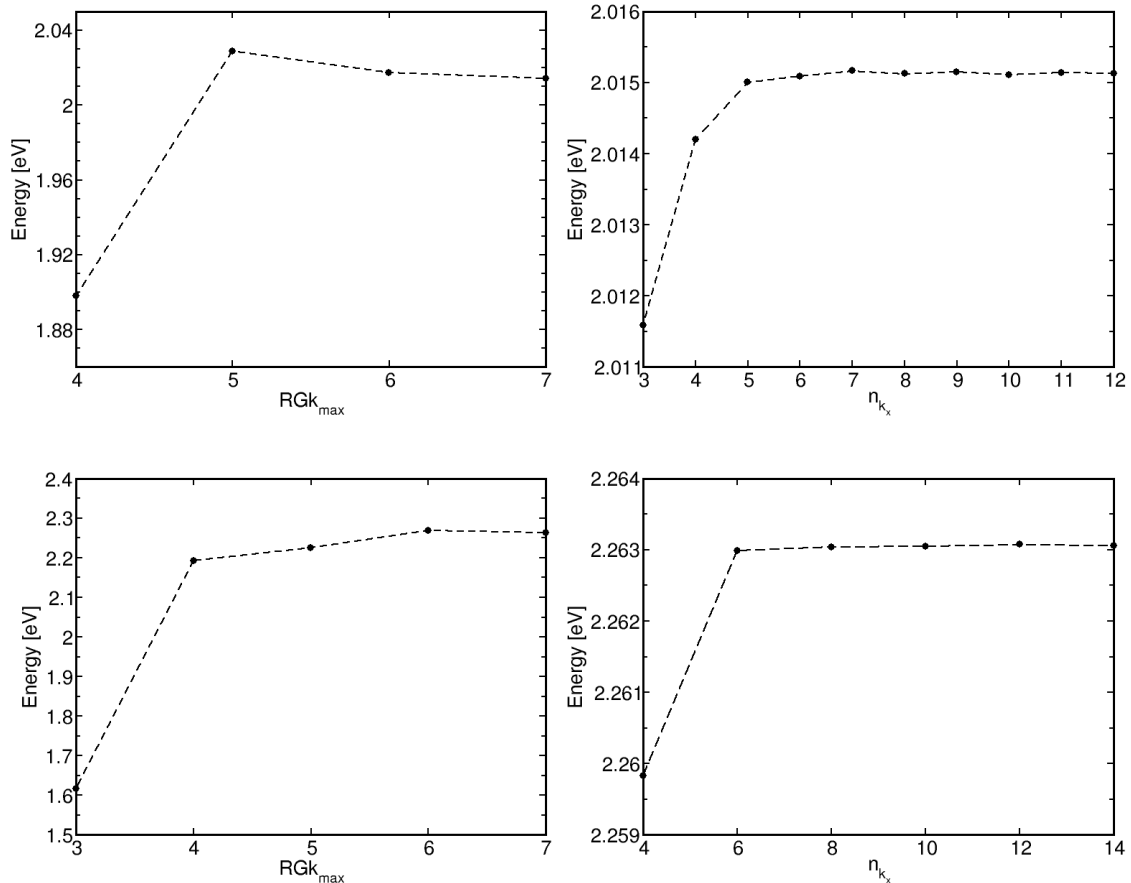
Figure 4.2: Convergence behavior of the DFT-PBE band gap for rutile (top) and anatase (bottom) obtained with respect to RGk_{max} and **k**-grid represented by the number of **k**-points in the k_x direction n_{k_x}.

for rutile and 2100 basis functions for anatase. In the muffin-tin spheres a spherical harmonics expansion up to $l = 10$ is taken into account. For rutile, the **k**-mesh is chosen to be $4 \times 4 \times 6$ which corresponds to 24 **k**-points in the irreducible wedge. For anatase, the mesh $6 \times 6 \times 2$ is chosen corresponding to 20 irreducible **k**-points.

4.2.2 Structure optimization with PBE

Using the initial experimental lattice parameters a structure optimization with respect to the total energy is performed. The optimization process entails alternating variation of two parameters – the unit-cell volume and the c/a ratio – until the parameters do not vary within a predefined accuracy, the convergence criteria. During the variation of one parameter the other is kept fixed. In each optimization step we obtain a number of total-energy data points corresponding to the generated deformed structures. In the case of volume optimization the Birch-Murnaghan equation of state is fitted to the total-energy data points to obtain the equilibrium volume and energy. In the case of c/a ratio optimization a fourth-order polynomial fit is used for calculating the equilibrium energy and the corresponding strain.

Convergence criteria of $0.01\,\text{Å}^3$ for the unit-cell volume and 10^{-4} for the c/a

ratio are used. After a four step optimization procedure the lattice parameters of $a = b = 4.5991\,\text{Å}$ and $c = 2.9257\,\text{Å}$ are obtained for rutile and $a = b = 3.7268\,\text{Å}$ and $c = 9.7433\,\text{Å}$ for anatase. The optimized parameters agree with the experimental ones to within 1% accuracy. We use the PBE-optimized unit-cell parameters for all subsequent calculations.

Even though the Kohn-Sham gap does not represent the correct fundamental band gap, we follow the common practice of discussing it. The rutile band gap obtained with PBE is 1.99 eV and direct at the Γ-point. The band gap is quite close to the recently reported DFT-PBE values of 1.88 eV by Landmann *et al.* [45] and 1.93 eV by Chiodo *et al.* [46]. Similar to the observations of Landmann *et al.* the local conduction band minima at the high symmetry points M and R lie only 0.04 eV and 0.02 eV, respectively, higher in energy than at the Γ-point. For anatase the Kohn-Sham band gap is 2.36 eV and also direct at Γ, whereas slightly lower indirect band gaps of 1.94 eV [45] and 2.15 eV [46] are reported.

4.2.3 Ground state with PBE0$'$

In PBE0$'$ calculations we examine the convergence with respect to the **k**-mesh and the number of unoccupied states N_{unocc} that enters the calculation through the exact exchange by means of Eq. (1.42). We note that in PBE0$'$ calculations we shift the **k**-mesh by a small vector in order to avoid **k**-points in high-symmetry directions. This serves to improve the numerical stability and convergence of the calculation.
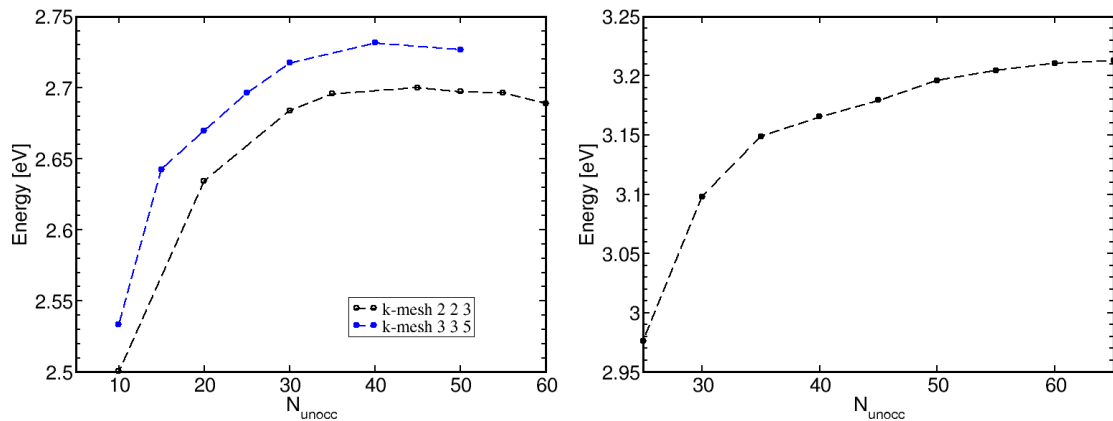
Figure 4.3: Convergence behavior of the DFT-PBE0$'$ band gap with respect to the number of unoccupied states and different **k**-meshes for rutile (left) and for the **k**-mesh $3 \times 3 \times 1$ for anatase (right).

The convergence tests for the band gap are presented in Fig. 4.3. We have to use a lower number of **k**-points in these calculations because of the bad time-scaling behavior of the exact exchange part. For rutile, we achieve an accuracy of 0.05 eV with the **k**-mesh $3 \times 3 \times 5$ and 50 unoccupied states. Then the PBE0$'$ band gap has the value of 2.73 eV and it is direct at the Γ point. The Γ-point is still almost degenerate with M and R points that are 0.03 eV and 0.06 eV higher in energy,

respectively. This band gap is larger than the PBE one by about 0.7 eV. The result follows the general tendency of hybrid functionals to increase the band gap compared to local or semilocal exchange-correlation functionals [62].

For anatase, a full self-consistency field calculation can be performed with the **k**-mesh $3 \times 3 \times 1$ only. This makes it difficult to estimate the accuracy of the result: The band gap is converged to 3.21 eV with respect to the number of unoccupied states for $N_{unocc} = 60$ within the accuracy of 0.01 eV, however the **k**-point sampling causes larger fluctuations judging from the investigation of rutile. We cautiously assume that the convergence behavior is similar to the case of rutile, and the accuracy lies within $0.05 - 0.1$ eV. The obtained band gap of 3.2 eV that is direct at Γ looks reasonable comparing the PBE-PBE' band-gap shift of rutile (0.7 eV) to that of anatase (0.9 eV).

4.3 G_0W_0 calculations

We now address the quasi-particle corrections of DFT energy levels conducted employing the G_0W_0 approximation on top of PBE as well as PBE0' calculations. There are several computational parameters that are essential to the convergence of the results. The results are most difficult to converge with respect to the number of **k**-points for the Brillouin-zone integration. Further, a summation over the number of unoccupied states N_{unocc} is required in the calculation of the self-energy and polarization. To understand the other parameters, we have to briefly speak of the basis set in G_0W_0 calculations. When evaluating the G_0W_0 equations (2.45)-(2.49) with the chosen Green function G_0 (Eq. (2.50)), products of two Kohn-Sham functions arise. In order to reformulate the equations in a matrix form, these products are expanded in a so-called *mixed* basis that is constructed within the APW+lo framework. The radial functions in the muffin-tin spheres are constructed from products of APW+lo radial functions. The latter are taken into account up to the cut-off angular momentum l_{MB}. In the interstitial the mixed basis is constructed from plane waves. The resulting plane wave expansion is truncated at G_{max}^{MB}. We characterize it by the quantity $G_{MB} = G_{max}^{MB}/G_{max}$ with G_{max} corresponding to the APW+lo cut-off for the interstitial basis functions. Thus, the parameters l_{MB} and G_{MB} determine the quality of the mixed basis set. Another parameter that impacts the accuracy is N_ω, the number of frequency points for the integration over the frequency axis in the calculation of the self-energy. The integration is carried out using the Gauss-Legendre scheme where the integral is split into two parts separated at ω_0. The G_0W_0 implementation containing a detailed description of these convergence parameters is given in [32].

The convergence tests for rutile are presented in Fig. 4.4 for the direct band gap at Γ. For every test the following parameters are used except for the ones being varied: **k**-mesh $3 \times 3 \times 5$, $N_{unocc} = 200$, $l_{MB} = 2$, $G_{MB} = 0.8$, and $N_\omega = 20$ with $\omega_0 = 1$ eV. Relatively small values of $l_{MB} = 2$ and $G_{MB} = 0.8$ suffice to achieve the accuracy of 0.01 eV for the mixed basis set, the same applies to $N_\omega = 20$ with $\omega_0 = 1$ eV. Similarly $N_{unocc} = 300$ and the **k**-mesh $4 \times 4 \times 6$ suffices for the same accuracy. Thus, the direct band gap at Γ is 3.26 eV. Interestingly, when using the

mesh $4 \times 4 \times 6$ we obtain an indirect band gap of $3.16\,\mathrm{eV}$ between the valence band maximum at Γ and conduction band minimum along the path $X \to R$ near point R. The indirect band gap is $0.1\,\mathrm{eV}$ lower than the direct one. We recall that the PBE and PBE0′ calculations yield almost degenerate conduction band minima at Γ and R points. Here, we obtain either a direct or an indirect band gap depending on the **k**-mesh. Tests for denser **k**-meshes with otherwise lower parameters show the following: For the meshes $3 \times 3 \times 5$ and $5 \times 5 \times 8$ a direct band gap is calculated, the meshes $4 \times 4 \times 6$ and $6 \times 6 \times 9$ yield the described indirect band gap. We keep both values in mind when comparing the band gap to literature values in the next section.
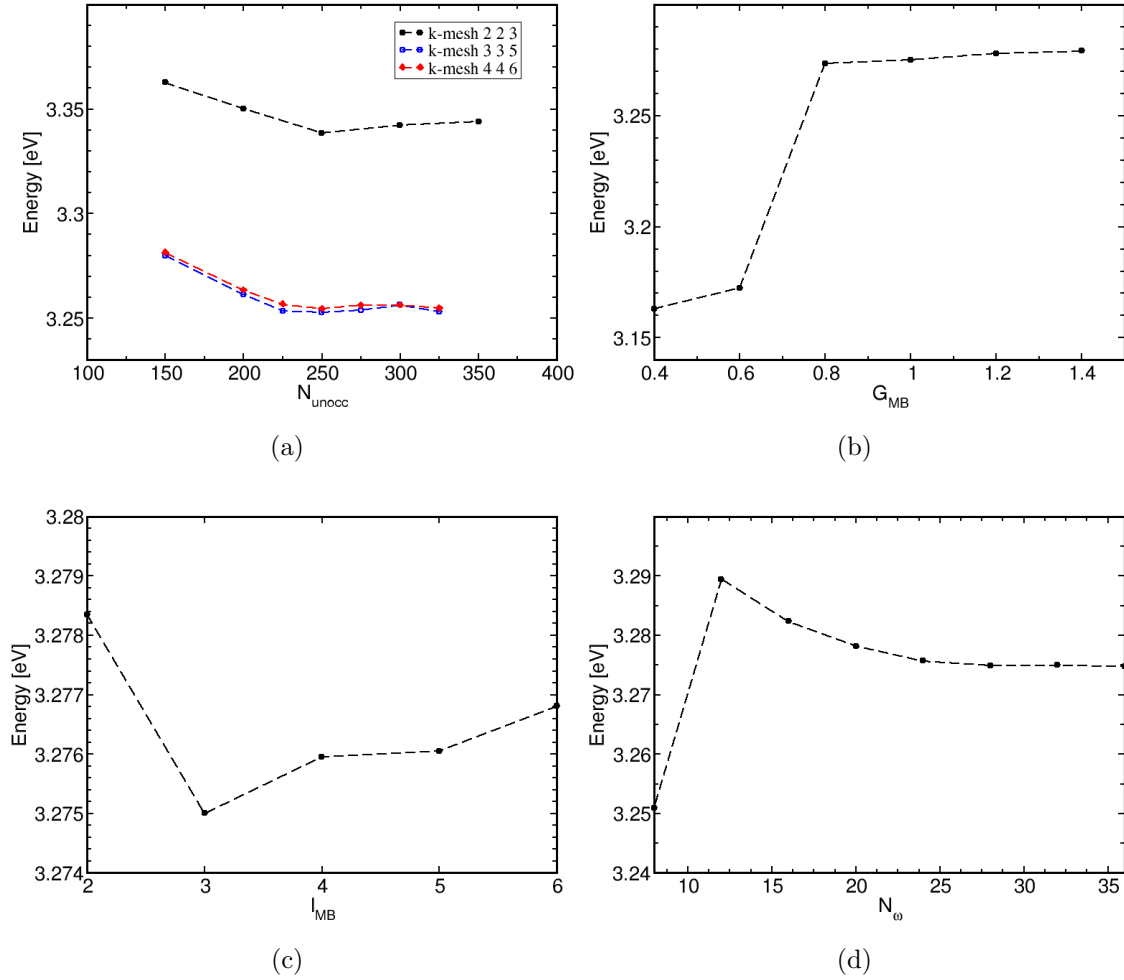
Figure 4.4: Convergence behavior of the direct band gap at Γ for rutile using G_0W_0 on top of PBE with respect to N_{unocc} for different **k**-meshes (a), the mixed basis parameters G_{MB} (b), and l_{MB} (c), and the number of points for the frequency integration N_ω (d).

The convergence tests for anatase are given in Fig. 4.5 for the direct band gap at Γ. We performed the tests using the following parameters except for the ones being varied: **k**-mesh $6 \times 6 \times 2$, $N_{unocc} = 200$, $l_{MB} = 2$, $G_{MB} = 0.8$, and $N_\omega = 20$ for $\omega_0 = 1\,\mathrm{eV}$. We see that the same mixed basis set and frequency integration parameters can be taken here as in the case of rutile: $l_{MB} = 2$, $G_{MB} = 0.8$, and

$N_\omega = 20$ with $\omega_0 = 1$ eV. Taking $N_{unocc} = 350$ and the **k**-mesh $6 \times 6 \times 2$ we obtain the band gap of 3.73 eV with the accuracy of 0.07 eV.
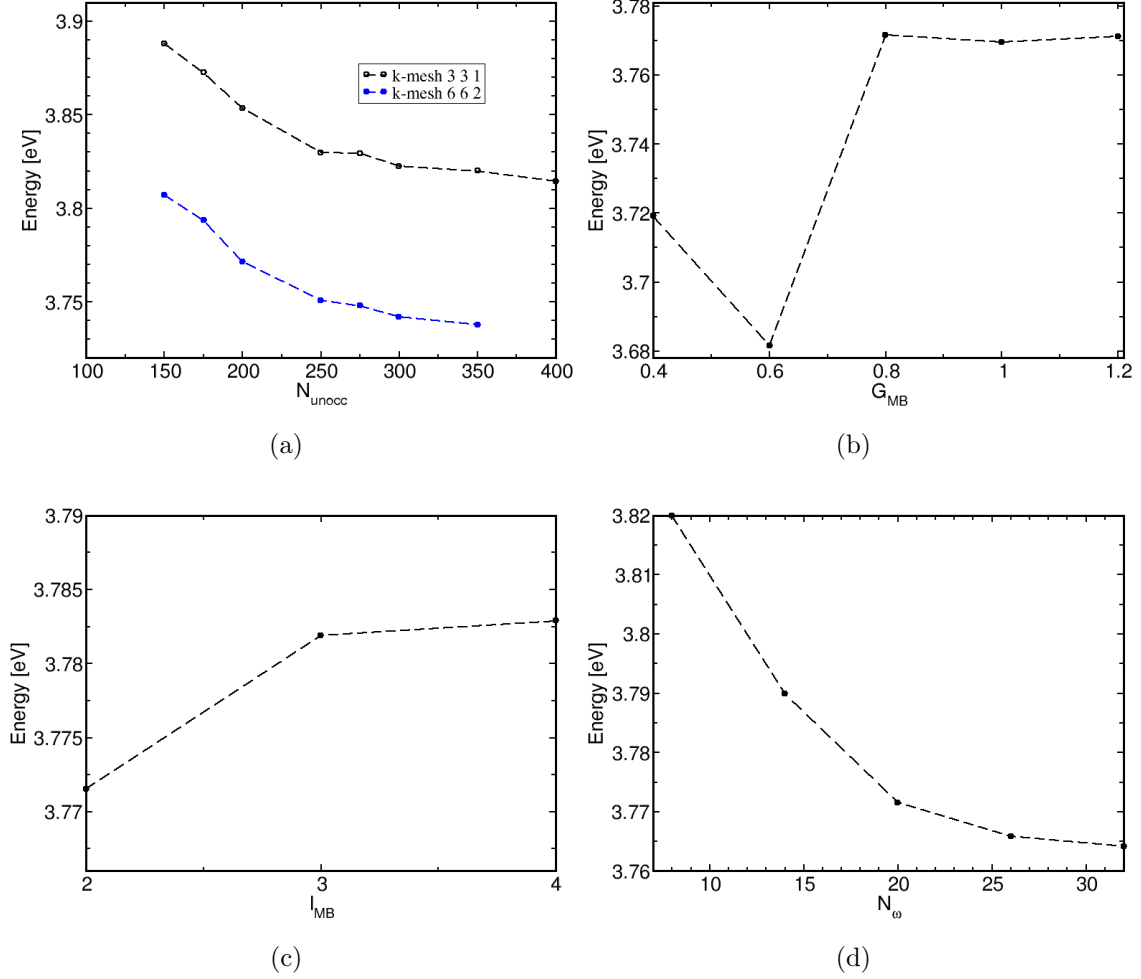

Figure 4.5: Convergence behavior of the direct band gap at Γ for anatase using G_0W_0 on top of PBE with respect to N_{unocc} for different **k**-meshes (a), the mixed basis parameters G_{MB} (b), and l_{MB} (c), and the number of points for the frequency integration N_ω (d).

Let us now discuss the G_0W_0 calculations on top of PBE0′. For implementation reasons the grids of the PBE0′ and G_0W_0 calculation have to be the same. Since the ground-state calculation could be performed only for smaller grids, we run one self-consistent cycle with a denser grid on top of the converged PBE0′ calculation. For the mixed basis and the frequency integration parameters the same values are determined as in the previously discussed calculations. We show the more problematic convergence tests for different **k**-meshes and N_{unocc} in Fig. 4.6. For rutile the indirect band gap between the valence band maximum at Γ and the conduction band minimum at R with the value of 3.39 eV is obtained. The parameters $N_{unocc} = 300$ and the **k**-mesh $4 \times 4 \times 6$ provide the accuracy of 0.05 eV. The local conduction band minimum at the point Γ lies only 0.06 eV higher than at the point R, so once more we cannot make a definitive statement as to nature of the band gap.

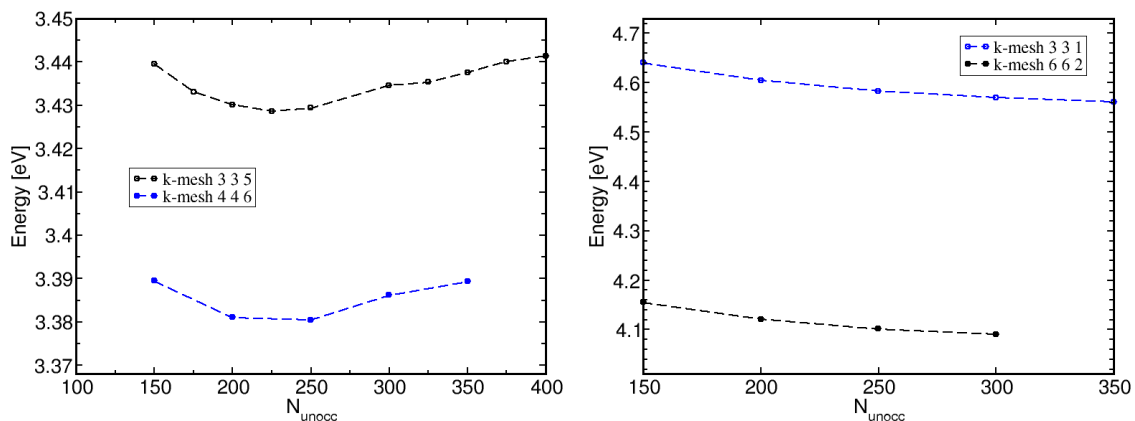For anatase, the convergence is poor with respect to the **k**-mesh. By choosing

Figure 4.6: Convergence behavior of the band gap using G_0W_0 on top of PBE0$'$ with respect to N_{unocc} and different **k**-meshes for rutile (left) and anatase (right). In case of rutile, the indirect band gap between the valence band maximum at Γ and the conduction band minimum at R is presented, in case of anatase the direct band gap at Γ is shown.

the mesh $6 \times 6 \times 2$ the band gap is lowered by $0.5\,\text{eV}$ compared to the mesh $3 \times 3 \times 1$. Unfortunately, we are unable to use a denser grid since the PBE0$'$ calculation on a $9 \times 9 \times 3$ mesh is too time-consuming to perform. Still, we expect the value to be closer to the converged one than 0.5 eV if we compare the results to rutile. G_0W_0 shifts the band gap of rutile by $0.7\,\text{eV}$ from the pure PBE0$'$ calculation, for anatase the shift constitutes 0.9 eV.

4.4 Band structure

In this section we summarize the results for the electronic band structure procured on different theory levels. The results for the electronic band gap of rutile are presented in Tab. 4.1. To our knowledge, there is no study of electronic structure of rutile or anatase using the same PBE0$'$ functional, so we can compare the G_0W_0@PBE0$'$ band gap only to experiment.

	This work	References
PBE	1.99	1.88 [45], 1.93 [46]
G_0W_0@PBE	3.16(I), 3.26	3.46 [45], 3.59 [46], 3.34(I) [47]
PBE0$'$	2.73	
G_0W_0@PBE0$'$	3.39(I)	
exp.		3.3 ± 0.5 [48], 3.6 ± 0.2 [49], 4.0 [50]

Table 4.1: Calculated band gaps in eV for rutile using different functionals compared to theoretical and experimental references. (I) indicates an indirect band gap.

The available experimental data is spread over a broad range. Tezuka *et al.* reported a band gap of 3.3 ± 0.5 eV [48] from combined photoemission and bremsstrahlung isochromat spectroscopy measurements. Rangan *et al.* [49] report a band

gap of 3.6 ± 0.2 eV from combined UPS and IPES for the rutile [110] surface. Furthermore a value of 4.0 eV was reported from angle-resolved photoemission experiments [50].

The band gaps at DFT level are considerably lower than the quasi-particle and experimental ones. This illustrates the effect of the exchange-correlation derivative discontinuity as well as the deficiencies of the respective exchange-correlation approximation. Our G_0W_0@PBE calculations yield a band gap that is $0.2-0.4$eV lower than the references. Direct band gaps by Chiodo *et al.* [46] and Landmann *et al.* [45] are reported as well as an indirect band gap by Kang *et al.* [47]. The reported indirect band gap is between the same high symmetry points (Γ and R) as in our calculation. Seeing that the experimental data lies in a wide range both G_0W_0@PBE and G_0W_0@PBE0$'$ calculations are in good agreement with the measurements.

Tab. 4.2 summarizes the results for anatase. The is no photoemission data on the fundamental band gap of anatase. An approximate assessment is nevertheless possible by considering that the direct electronic gap can not be lower than the direct optical gap of $3.7 - 3.9$ eV ([51, 52]). The value of the band gap for G_0W_0@PBE is

	This work	References
PBE	2.36	1.94(I) [45], 2.15(I) [46]
G_0W_0@PBE	3.7	3.73(I) [45], 3.83 (I) [46], 3.56(I) [47]
PBE0$'$	3.2	
G_0W_0@PBE0$'$	4.1	

Table 4.2: Calculated band gaps in eV for anatase using different functionals compared to theoretical and experimental references. (I) indicates an indirect band gap.

in good agreement with theoretical data, however in our case the band gap is direct whereas the reported band gaps are all indirect. Ref.[46, 47] report a band gap between a point close to X in the valence band and the Γ point in the conduction band. Our calculation is more in line with [45]: Their valence band maximum is along the path $\Gamma \rightarrow M$ near M, in our calculations this point is only 0.06 eV lower than the Γ point.

In light of the optical gaps of $3.7 - 3.9$ eV the G_0W_0@PBE gap may be too small. The G_0W_0@PBE0$'$ band gap of 4.1 eV is more in agreement with the data. Summarizing, we find that both G_0W_0@PBE and G_0W_0@PBE0$'$ prove to yield band gaps comparable to recent theoretical and experimental data.

In conclusion of this section, we present the quasi-particle band structure of rutile and anatase in Fig.4.7, along the high symmetry directions in the first Brillouin zone. The PBE and PBE0$'$ Kohn-Sham results are included to demonstrate the quasi-particle shift. For PBE, PBE0$'$, and G_0W_0@PBE$'$ the band structure is plotted using 100 $\mathbf{k}$-points for each band. The energy values for the $\mathbf{k}$-points are obtained by a Fourier interpolation scheme using the results of the respective ground-state or G_0W_0 calculation. In the case of G_0W_0@PBE there are too few $\mathbf{k}$-points for the interpolation to give reasonable results, so we display only these points. The valence band maximum is used as the zero point for the energy scale as it is located at the
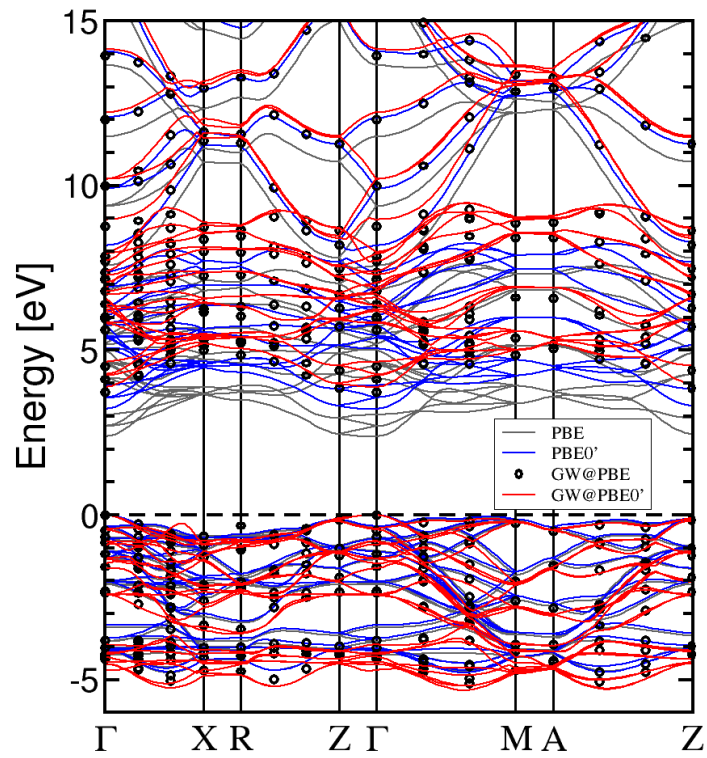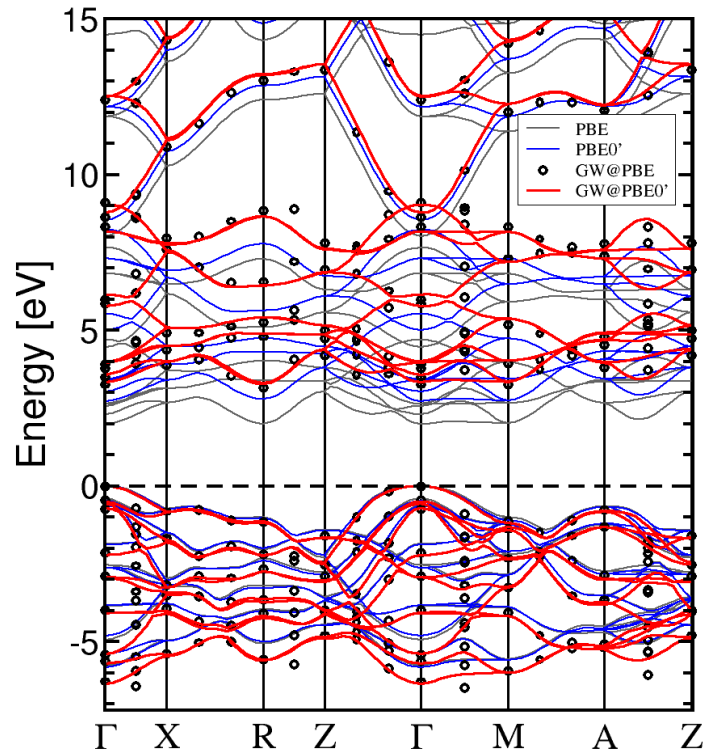
Figure 4.7: Electronic band structure of rutile (top) and anatase (bottom) along the high symmetry directions in the first Brillouin zone on different theory levels.

Γ-point for each calculation.

The valence states in both phases are predominantly formed of $2p$ oxygen states that are partially hybridized with titanium $3d$ states. The conduction band is mainly formed by $3d$ states of titanium. Due to the octahedral-type crystal field the unoccupied Ti $3d$ states split into two sub-bands: the lower lying threefold-degenerate t_{2g}-like and the higher lying two-fold degenerate e_g-like states.[45].

4.5   Optical absorption spectra

In this section we discuss the macroscopic dielectric function obtained by solving the BSE. The calculations are conducted on four different levels of theory – based on PBE, PBE0′, G_0W_0@PBE and G_0W_0@PBE0′. The quantities that enter a BSE calculation are the respective quasi-particle energies from G_0W_0 or Kohn-Sham energies from DFT calculations and the wave functions known at DFT level.

The most relevant computational parameters we have to converge are the **k**-mesh and the number of valence N_{val} and unoccupied states N_{unocc} that determine the size of the BSE Hamiltonian 2.93. The parameters enter the calculation with the third power if the full Hamiltonian is diagonalized, so the calculation grow extremely demanding very fast. Furthermore, local-field effects are included by setting a cut-off parameter $|\mathbf{G}|_{max}$ so that the **G** are selected to lie within the cut-off.

Finally the number of unoccupied states that enter the calculation of the microscopic dielectric function which serves to calculate the screened Coulomb interaction has to be converged. A Lorentzian broadening of 0.1 eV is used for all spectra in the summation over the exciton states λ in Eq. (2.103) for the calculation of the dielectric function in order to smear out effects of the finite **k**-point sampling. The **k**-grid is shifted by a small vector in a direction different from the high-symmetry directions of the crystal, so that a maximum number of non-equivalent **k**-points can be used to achieve a better sampling.

Our results are comprised of the imaginary part of the dielectric function for the light polarization along the axes a, b and c of the crystal. The spectra along a and b are equivalent because of the symmetry of rutile and anatase. We will refer to spectra with the light polarization perpendicular to the c axis as the in-plane component, and to those with the light polarization parallel to the c axis as the out-of-plane component.

First we perform convergence tests for different starting points investigating the singlet channel. The convergence tests with PBE as a starting point are presented in Fig. 4.8 taking the parameters $4 \times 4 \times 6$ mesh, $N_{val} = 13$, $N_{unocc} = 15$ and $N_{\mathbf{G}} = 63$ unless they are varied. Based on the tests we choose the spectra with the mesh $4 \times 4 \times 6$, $N_{val} = 12$, $N_{unocc} = 13$ and $63\,\mathbf{G}$ vectors. For the screening 20 unoccupied states are found sufficient.

We do not show the convergence tests for the parameters N_{val}, N_{unocc} and $N_{\mathbf{G}}$ when taking the functional PBE0′ and G_0W_0 calculations as a starting point as they all exhibit a very good convergence with the PBE values. However, we find that the
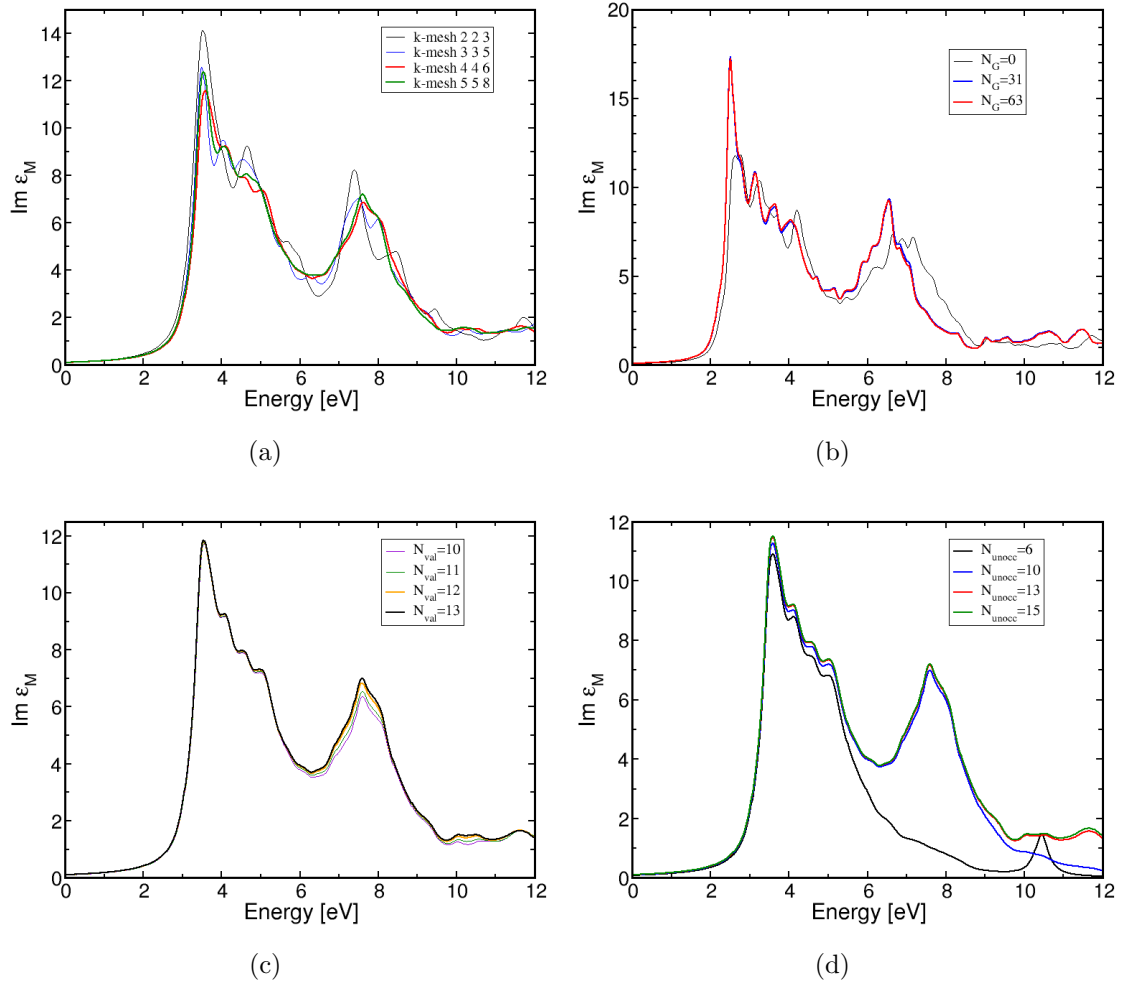
Figure 4.8: Convergence tests of the imaginary part of the macroscopic dielectric function for rutile on top of PBE with respect to the **k**-mesh (a), number of **G** vectors (b), number of valence bands N_{val} (c) and number of unoccupied bands N_{unocc} (d). The in-plane component of the singlet channel is shown.

k-grid sampling is more difficult to converge. The tests are shown in Fig. 4.9 and Fig. 4.10. For G_0W_0 the main peak positions and respective oscillator strengths do not change significantly for both grids. In case of PBE0′ the oscillator strength of both peaks are greatly increased when going form grid $2 \times 2 \times 3$ to $3 \times 3 \times 5$. The resulting spectrum is comparable to the G_0W_0@PBE0′ spectrum that is shifted to lower energies.

Utilizing the obtained computational parameters we compute the macroscopic dielectric function on different approximation levels of the BSE Hamiltonian as described in Section 2.3.5: the independent particle approximation (IP), the random-phase approximation (RPA) containing local field effects and the singlet and triplet channels (see Fig. 4.11). As a starting point the quasi-particle calculations are used. We observe that the optical absorption spectrum for the simplest approximation – that of the independent electron and hole – yields dramatically different results compared to the inclusion of excitonic effects. The absorption onset is found at
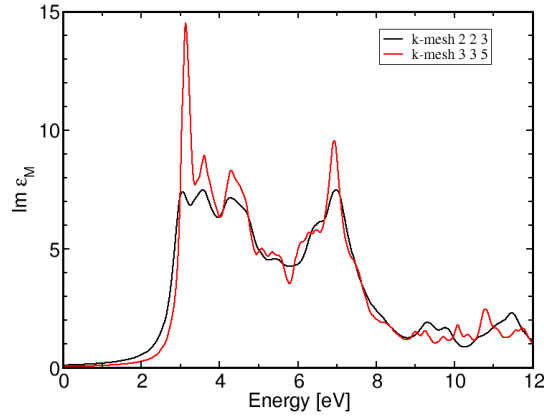
Figure 4.9: Convergence test of the imaginary part of the macroscopic dielectric function for rutile on top of PBE0′ with respect to the **k**-mesh. The in-plane component of the singlet channel is shown.
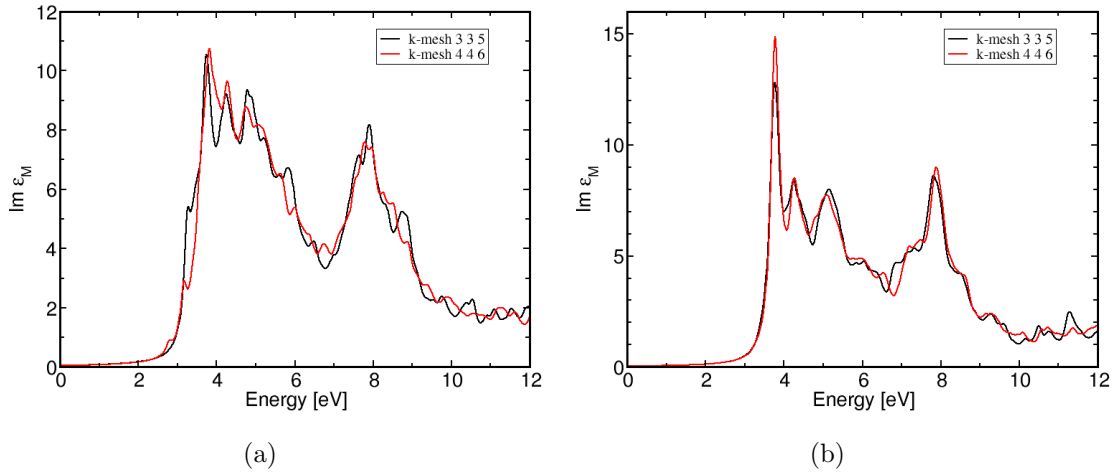

(a)   (b)

Figure 4.10: Convergence test of the imaginary part of the macroscopic dielectric function for rutile on top of G_0W_0@PBE (a) and G_0W_0@PBE0′ (b) with respect to the **k**-mesh. The in-plane component of the singlet channel is shown.

higher energies (approximately 4 eV), the oscillator strengths are underestimated. The inclusion of local field-effects in the RPA approximation does not alter the features significantly. Looking at the singlet result we observe that the attractive screened Coulomb interaction shifts the spectrum to lower energies by about 1 eV and redistributes the oscillator strength towards lower energy peaks. The spectrum is completely altered from the IP and RPA cases. Comparing singlet and triplet we find no significant changes for G_0W_0@PBE. In case of G_0W_0@PBE0′ the second peak is shifted to slightly lower energies for the triplet channel.

In the following we are interested in the singlet channel, since we can compare it to theoretical and experimental data in the literature. Let us first discuss the singlet spectra calculated from different starting points in Fig. 4.12. It is evident that the absorption edge is shifted in energy according to the band gap value produced by different starting points. Going from PBE0 to G_0W_0@PBE0′ we see that the
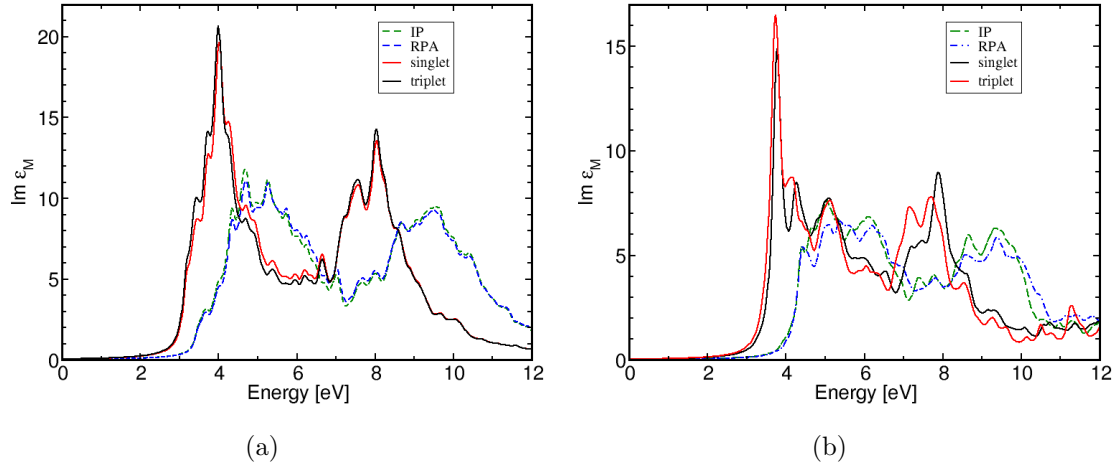
(a)   (b)

Figure 4.11: Imaginary part of the macroscopic dielectric function for rutile using different approximation levels for the BSE Hamiltonian with G_0W_0@PBE (out-of-plane component) (a) and G_0W_0@PBE0′ (b) (in-plane component) as starting points.
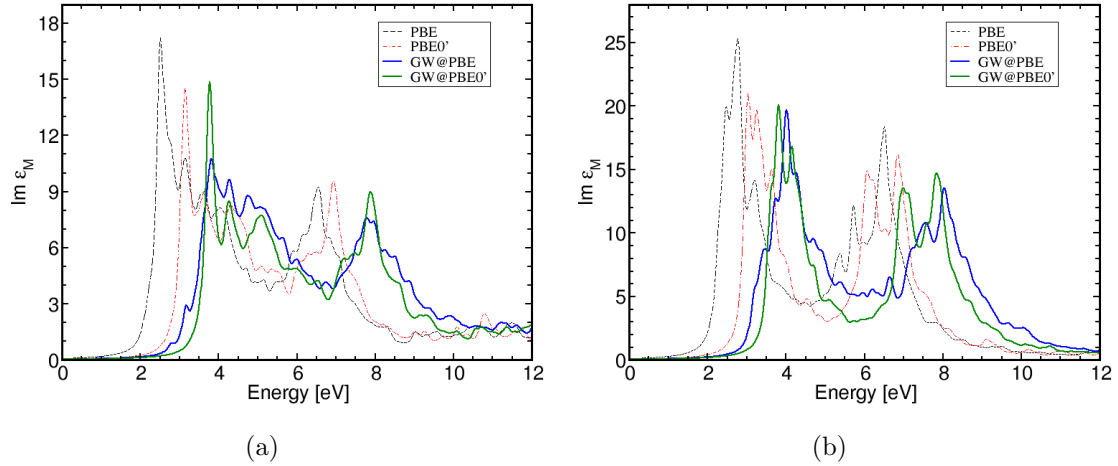

(a)   (b)

Figure 4.12: Imaginary part of the macroscopic dielectric function for rutile on different theory levels for the in-plane (a) and out-of-plane (b) components. The singlet channel is shown.

oscillator strength of the first peak is greatly reduced, especially in the case of in-plane polarization. The oscillator strength is redistributed in such a way that a clear absorption edge is not visible, instead we observe the formation of several small features before the first main absorption peak. We presume that the artifact is mostly related to the G_0W_0 band energies and the insufficiency of the interpolation algorithm between the calculated **k**-points. Going from PBE0′ to G_0W_0@PBE0′ does not reduce the oscillator strength significantly, the shape of the spectrum is mostly preserved.

As a next step we compare the spectra @G_0W_0 to the available theoretical and experimental data. G_0W_0@PBE0′ is generally in better agreement with the experimental data than G_0W_0@PBE. The absorption edge of the first excitonic peak at about 3.5 eV is reproduced well by G_0W_0@PBE0′ for both components. Slight devi-

ation of the peak position of about $0.2 - 0.3$ eV is observed in the direction of lower energies whereas other theoretical data tend to shift the peak to higher energies. The differences in the calculated band gap are responsible for this variation. For
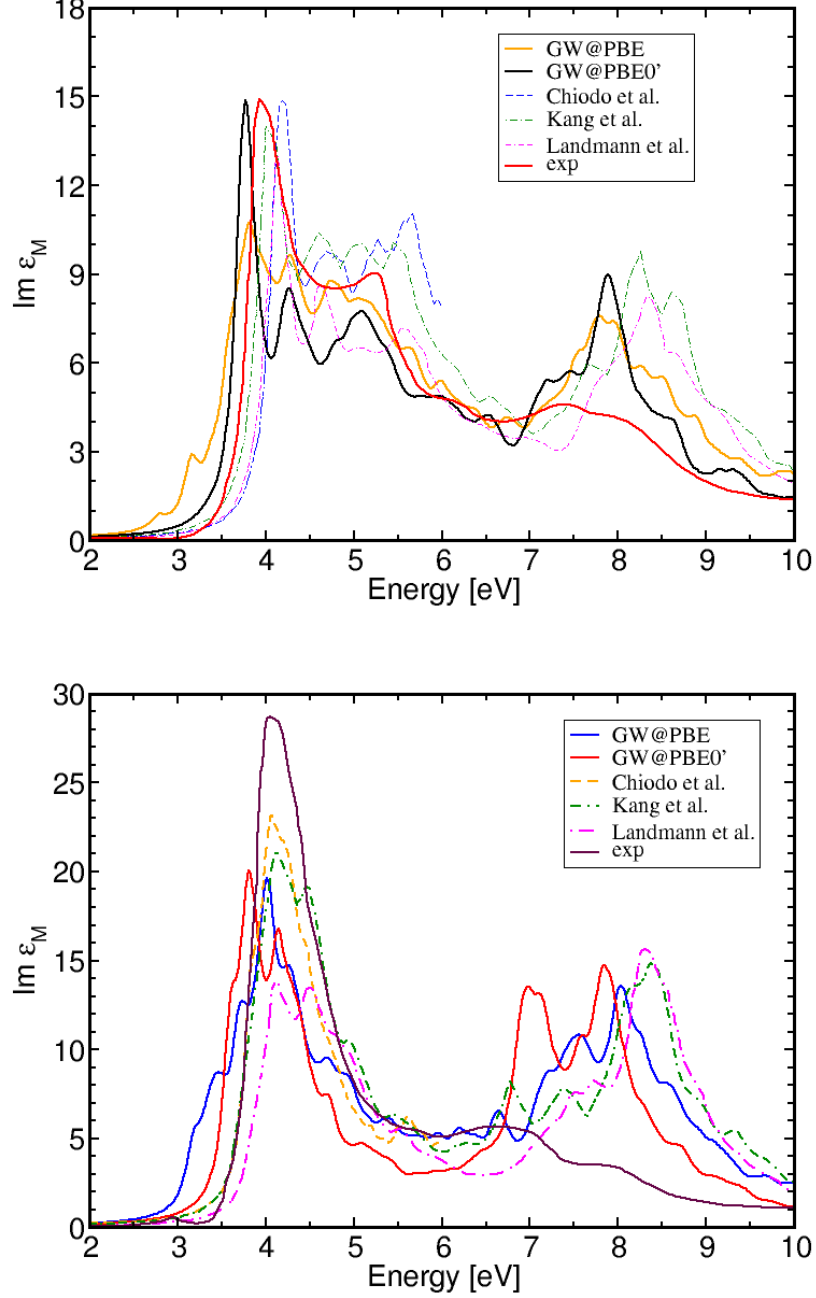

Figure 4.13: The in-plane (top) and out-of-plane (bottom) components of the imaginary part of the macroscopic dielectric function for rutile compared to theoretical spectra calculated by Chiodo *et al.* [46], Landmann *et al.* [45] and Kang *et al.* [47]. The experimental data is taken from Cardona *et al.* [53].

the in-plane component the peak intensity is perfectly reproduced by G_0W_0@PBE0′, and underestimated by G_0W_0@PBE. In the out-of-plane polarization all of the theoretical data predict lower intensity than seen in the experiment. Furthermore, the

theoretical data predict a second major peak in the higher energy region above 6.5 eV that is not resolved in this intensity by the experiment. However, more recent experimental data by Tiwald *et al.* [54] indicate the existence of the major peak at ~ 8 eV for both polarizations [45], so the experimental data is controversial on that account.

We now turn to the absorption spectra of anatase. The convergence tests for the singlet channel with PBE as a starting point are presented in Fig. 4.14 taking the parameters $6 \times 6 \times 2$ mesh, $N_{val} = 23$, $N_{unocc} = 22$ and $N_{\mathbf{G}} = 119$ unless they are varied. 30 unoccupied states are taken into account for the screening. Based on the tests we choose these parameters for further calculations.
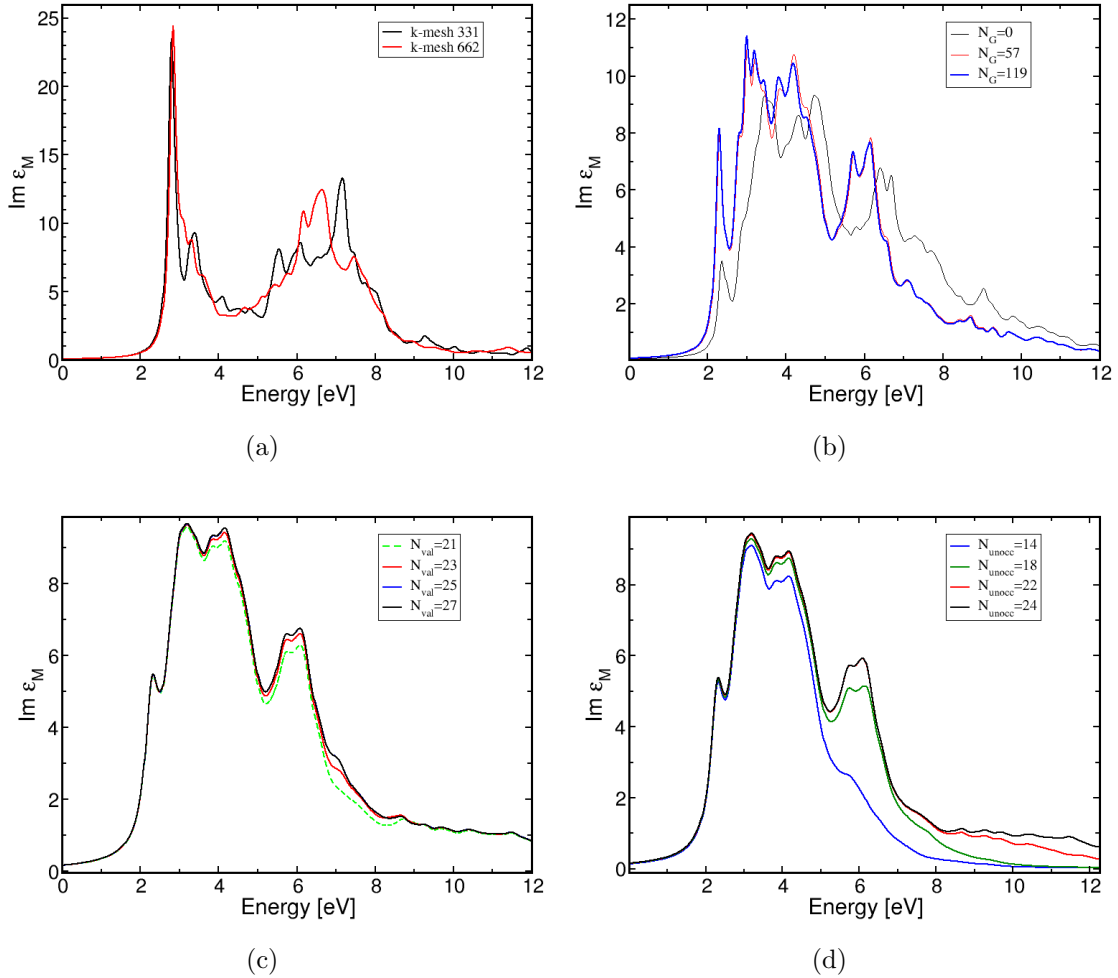

Figure 4.14: Convergence tests of the imaginary part of the macroscopic dielectric function for anatase on top of PBE with respect to the **k**-mesh (a), number of **G** vectors (b), number of valence bands N_{val} (c) and number of unoccupied bands N_{unocc} (d). The out-of-plane component of the singlet channel is shown in (a), (b)-(d) present the in-plane components of the singlet channel.

The convergence test for G_0W_0@PBE with respect to the **k**-grid is shown in Fig. 4.15. The are still some differences concerning the intensity distribution when going to the denser grid, however the major shape does not change.

Since the necessary ground-state PBE0′ calculation could not be performed on the grid $6 \times 6 \times 2$ we have to take the grid $3 \times 3 \times 1$ for PBE0′ and G_0W_0@PBE0′ keeping in mind that it is not well converged.
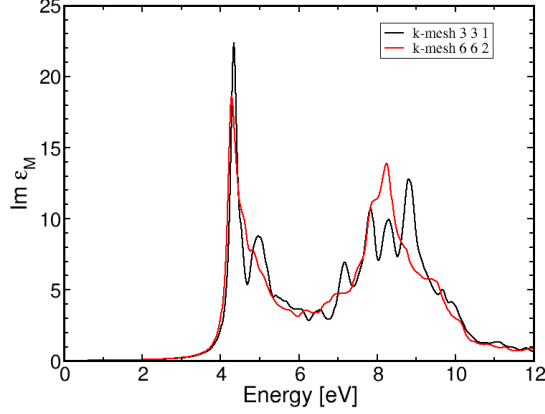

Figure 4.15: Convergence test of the imaginary part of the macroscopic dielectric function for anatase on top of G_0W_0@PBE with respect to the **k**-mesh. The out-of-plane component of the singlet calculation is shown.

Let us look at the different approximation levels of the BSE Hamiltonian in Fig. 4.16 using the quasi-particle calculations as a starting point. As in the case

<div align="center">(a)</div>

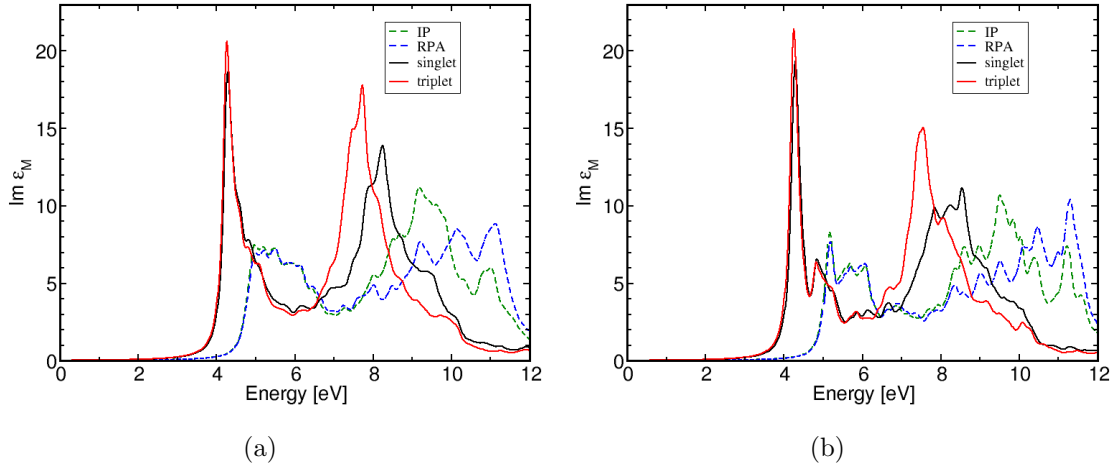

<div align="center">(b)</div>

Figure 4.16: Imaginary part of the macroscopic dielectric function for anatase using different approximation levels for the BSE Hamiltonian with the G_0W_0@PBE (a) and G_0W_0@PBE0′ (b) as starting points both in the out-of-plane polarization.

of rutile the spectrum is overall changed by including the excitonic effects. The shift of the absorption edge to lower energies in singlet and triplet channels and the appearance of a sharp peak at 4 eV indicate a large excitonic effect. When comparing IP and RPA approximations we observe that the local-field effects have a noticeable effect in the higher energy part of the spectrum starting from $\sim 8\,\mathrm{eV}$: They shift the oscillator strengths to higher energies. The same effect is found comparing singlet and triplet channels. The triplet peak above $\sim 7\,\mathrm{eV}$ is blueshifted by $\sim 0.8\,\mathrm{eV}$. The

comparison of the independent-particle and the drastically changed full interacting BSE spectrum prove the need to include excitonic effects in our calculations.

The comparison of singlet spectra from different ground-state starting points is depicted in Fig. 4.17. Once more we observe the shift of the absorption edge corresponding to the respective band gap. A sharp absorption onset is found at 3.5eV and 3.8 eV in the in-plane component for G_0W_0@PBE and G_0W_0@PBE0′, respectively. For the out-of-plane component the first peak coincides for the quasi-particle calculations at 4 eV and the higher lying ones differ only in the oscillator strength. The intensity is slightly lowered going from PBE0′ to G_0W_0@PBE0′ calculation for both components. Going from PBE to G_0W_0@PBE calculation the intensity remains the same or is even increased.
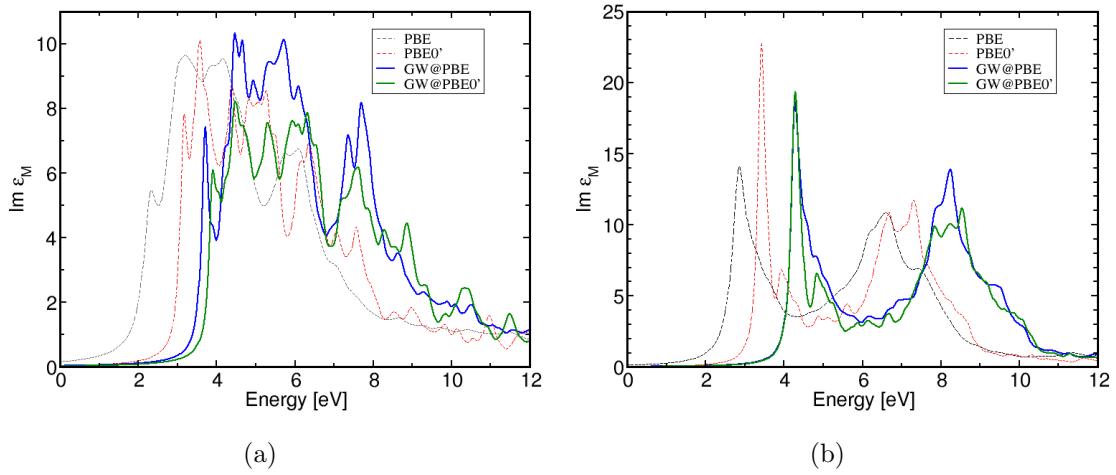

Figure 4.17: Imaginary part of the macroscopic dielectric function for anatase on different theory levels for the in-plane (a) and out-of-plane (b) components. The singlet channel is displayed.

Comparing the quasi-particle spectra to the experimental results for the out-of-plane polarization we see that the positions of the peak at the absorption edge at 4 eV as well as the higher energy peak at ~ 8 eV are remarkably well-described by both G_0W_0@PBE and G_0W_0@PBE0′. However, the intensity of both peaks are overestimated which is also the result of theoretical curves in the literature. Comparing the in-plane components, only G_0W_0@PBE0′ matches the experimental absorption onset exactly, the G_0W_0@PBE spectrum is slightly redshifted by 0.3 eV. However, G_0W_0@PBE gives correct oscillator strength, whereas the intensity of the first broad peak is underestimated by G_0W_0@PBE0′. The second peak in the energy region $7 - 8$ eV is reproduced energetically, but the intensity is overestimated by all presented theoretical spectra.

To summarize, the results indicate for both phases two absorption peaks that can be either sharp or broad: The first is located at the absorption onset and the second above 6.5 eV. The distribution reflects the interband transitions from the valence band to crystal-field split conduction bands. The energetically lower peak corresponds to transition from the valence band into the t_{2g} sub-band and the higher peak corresponds to transitions into the e_g sub-band. The results indicate that the

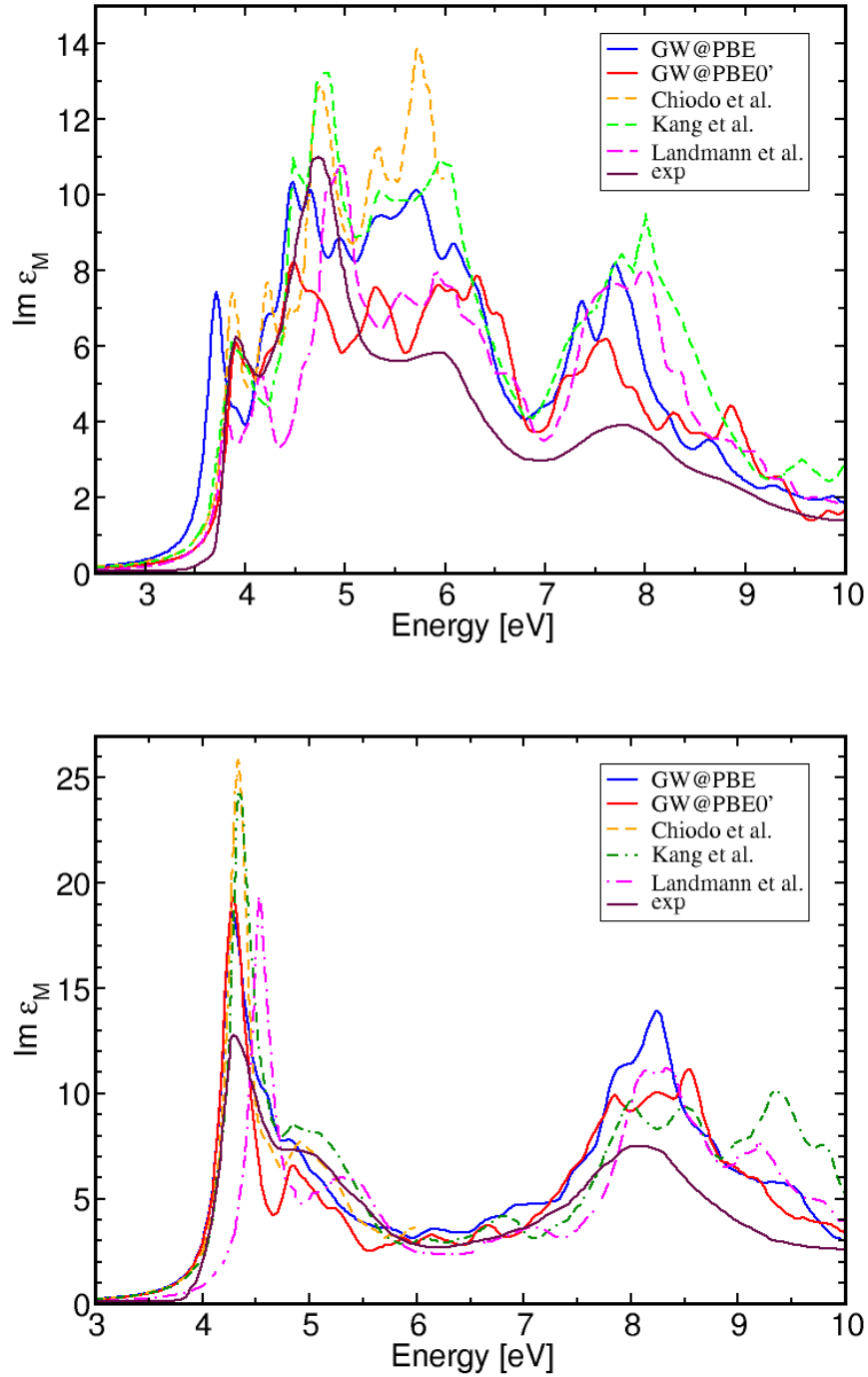electronic band gap as well as the optical transitions are mostly well-described by the many-body effects.

Figure 4.18: The in-plane (top) and out-of-plane (bottom) components of the imaginary part of the macroscopic dielectric function for anatase compared to theoretical spectra calculated by Chiodo *et al.* [46], Landmann *et al.* [45] and Kang *et al.* [47]. The experimental data is taken from Hosaka *et al.* [55].

Conclusions and outlook

In the present work we have investigated the electronic and optical properties of rutile and anatase phases of TiO_2. The fundamental band gaps obtained by G_0W_0 quasi-particle corrections were found to be generally in good agreement with the available theoretical data. Due to the wide range or a lack of experimental data, we can not determine whether the G_0W_0@PBE or the G_0W_0@PBE0$'$ approach performs better as a starting point. Using the hybrid PBE0$'$ functional as a starting point yields larger band gaps, the energy differences are about $0.2 - 0.4$ eV compared to the PBE starting point. This has a direct influence on the absorption edge of the optical spectrum. We observed that the G_0W_0@PBE0$'$ spectra are mostly blueshifted compared to the G_0W_0@PBE ones. Ideally, the application of MBPT should yield band structures independent of the ground-state starting point. However, it is not possible considering the approximations made in the derivation of G_0W_0. An improvement upon the situation may be achieved by performing a self-consistent or a partially self-consistent GW calculation and taking the neglected terms of the vertex function into account. This would come at a significantly increased computational cost.

The qualitative features of experimental absorption spectra could be reproduced employing both exchange-correlation potentials. There are, however, quantitative differences concerning peak intensities and positions for both phases and light polarizations. The differences in the band structure attribute strongly to these deviations. We also take into account that some PBE0$'$ calculations could not be well converged due to the computation time. Very good convergence with respect to the $\mathbf{k}$-grid could not achieved in all cases as the size of the BSE eigenvalue problem constitutes a bottleneck of the computation.

A further significant issue that may attribute to quantitative differences between our results and the experiment is the neglect of the electron-phonon coupling present in the experimental spectra. The excited-states calculations are conducted on a frozen lattice so that no possible relaxation effects are accounted for. Forces shall be implemented within BSE formalism in future research.

Currently we research a conceptually different approach to determine the optical properties of materials, the so-called constrained density functional theory. The goal is to obtain optical excitations without having to invoke the computationally expensive machinery of the many-body perturbation theory. Within this method, we attempt to manipulate the occupation numbers of Kohn-Sham orbitals in a way that emulates a neutral excitation. The idea is to account for the electron-hole ef-

fects through the constraint of occupation numbers on DFT level, and subsequently perform the calculation of the dielectric function in the independent-particle approximation. In the best case scenario individual excitons would be accessible through this procedure.

Bibliography

[1]   HOHENBERG, P. ; KOHN, W.: In: *Phys. Rev.* 136 (1964), B864 S.

[2]   AMBROSCH-DRAXL, C. ; SAGMEISTER, S. ; MEISENBICHLER, Ch. ; SPITALER, J.: *EXCITING code.* [online] http://exciting-code.org, 2009

[3]   LEVY, M.: In: *Phys. Rev. A* 26 (1982), 1200 S.

[4]   DREIZLER, R. M. ; GROSS, E. K. U.: *Density Functional Theory.* Springer Verlag, Berlin, 1990

[5]   KOHN, W. ; SHAM, L. J.: In: *Phys. Rev.* 140 (1965), A1133 S.

[6]   FIOLHAIS, C. ; NOGUEIRA, F. ; MARQUES, M. A. L.: *A Primer in Density Functional Theory.* Springer Verlag, Berlin, 2003

[7]   CEPERLY, D. M. ; ALDER, B. J.: In: *Phys. Rev. Lett.* 45 (1980), 566 S.

[8]   PERDEW, J. P. ; WANG, Y.: In: *Phys. Rev. B.* 45 (1992), 13244 S.

[9]   PERDEW, J. P. ; ZUNGER, A.: In: *Phys. Rev. B.* 23 (1981), 5048 S.

[10] YIN, M. T. ; COHEN, M. L.: In: *Phys. Rev. Lett.* 45 (1980), 1004 S.

[11] LANGRETH, D. C. ; PERDEW, J. P.: In: *Phys. Rev. B* 21 (1980), 5469 S.

[12] PERDEW, J. P. ; BURKE, K. ; ENZERHOF, M.: In: *Phys. Rev. Lett.* 77 (1996), 3865 S.

[13] SHARP, R. T. ; HORTON, G. K.: In: *Phys. Rev.* 90 (1953), 317 S.

[14] TALMAN, J. D. ; SHADWICK, W. F.: In: *Phys. Rev. A* 14 (1976), 36 S.

[15] KRIEGER, J. B. ; LI, Y. ; IAFRATE, G. J.: In: *Phys. Rev. A* 45 (1992), 101 S.

[16] JANAK, J. F.: In: *Phys. Rev. B* 18 (1978), 7165 S.

[17] LEVY, M. ; PERDEW, J. P. ; SAHNI, V.: In: *Phys. Rev. A* 30 (1984), 2745 S.

[18] ALMBLADH, C.-O. ; BARTH, U. von: In: *Phys. Rev. B* 31 (1985), 3231 S.

[19] GODBY, R. W. ; SCHLÜTER, M. ; SHAM, L. J.: In: *Phys. Rev. B* 36 (1987), 6497 S.

[20] KNORR, W. ; GODBY, R. W.: In: *Phys. Rev. Lett.* 68 (1992), 639 S.

[21] FETTER, A. L. ; WALECKA, H. D.: *Quantum Theory of Many-Particle Systems.* McGraw-Hill, 1971

[22] STRINATI, G.: In: *Riv. Nuovo Cimento* 11 (1988), 1 S.

[23] MATTUCK, R. D. ; THEUMANN, A.: In: *Adv. Phys.* 20 (1971), 721 S.

[24] SCHWINGER, J.: In: *Proc. Nat. Acad. Sci. U.S.A.* 37 (1951), 452 S.

[25] MARTIN, P. ; SCHWINGER, J.: In: *Phys. Rev.* 115 (1959), 1342 S.

[26] BAYM, G.: In: *Phys. Rev.* 127 (1962), 1391 S.

[27] BAYM, G. ; KADANOFF, L. P.: In: *Phys. Rev.* 124 (1961), 287 S.

[28] HEDIN, L.: In: *Phys. Rev.* 139 (1965), A796 S.

[29] HEDIN, L. ; LUNDQUIST, S.: In: *Solid State Physics* 23 (1969)

[30] HYBERTSEN, M. S. ; LOUIE, S. G.: In: *Phys. Rev. B* 34 (1986), 5390 S.

[31] HYBERTSEN, M. S. ; LOUIE, S. G.: In: *Phys. Rev. Lett.* 55 (1985), 1418 S.

[32] JIANG, H. ; GÓMEZ-ABAL, R. I. ; LI, X. ; MEISENBICHLER, C. ; AMBROSCH-DRAXL, C. ; SCHEFFLER, M.: In: *Computer Physics Communications* 184 (2013), 348 S.

[33] ADLER, S. L.: In: *Phys. Rev.* 126 (1962), 413 S.

[34] WISER, N.: In: *Phys. Rev.* 129 (1963), 62 S.

[35] AMBEGAOKAR, V. ; KOHN, W.: In: *Phys. Rev.* 117 (1960), 423 S.

[36] ROHLFING, M. ; LOUIE, S. G.: In: *Phys. Rev. B* 62 (2000), 4927 S.

[37] ALBRECHT, S. ; REINING, L. ; DEL SOLE, R. ; ONIDA, G.: In: *Phys. Rev. Lett.* 80 (1998), 4510 S.

[38] BECHSTEDT, F. ; TENELSEN, K. ; ADOLPH, B. ; DEL SOLE, R.: In: *Phys. Rev. Lett.* 78 (1997), 1528 S.

[39] PUSCHNIG, P.: *Excitonic Effects in Organic Semi-Conductors - An Ab-initio Study within the LAPW Method*, University Graz, Diss., 2002

[40] SLATER, J. C.: In: *Phys. Rev.* 51 (1937), 846 S.

[41] SJÖSTEDT, E. ; NORDSTRÖM, L. ; SINGH, D. J.: In: *Sol. Stat. Comm.* 114 (2000), 15 S.

[42] SINGH, D.: In: *Phys. Rev. B* 43 (1991), Nr. 8, 6388–6392 S.

[43] Meagher, E. P. ; Lager, G. A.: In: *The Canadian Mineralogist* 17 (1979), 77 S.

[44] Parker, R. L.: In: *Zeitschrift für Kristallographie, Kristallgeometrie, Kristall-physik, Kristallchemie (-144,1977)* 59 (1924), 1 S.

[45] Landmann, M. ; Rauls, E. ; Schmidt, W. G.: In: *J. Phys.: Condens. Matter* 24 (2012), 195503 S.

[46] Chiodo, L. ; García-Lastra, J. M. ; Iacomino, A. ; Ossicini, S. ; Zhao, J. ; Petek, H. ; Rubio, A.: In: *Phys. Rev. Lett.* 82 (2010), 045207 S.

[47] Kang, W. ; Hybertsen, M. S.: In: *Phys. Rev. B* 82 (2010), 085203 S.

[48] Tezuka, Y. ; Shin, S. ; Ishii, T. ; Ejima, T. ; S., Suzuki ; Sato, S.: In: *J. Phys. Soc. Jpn.* 63 (1994), 347 S.

[49] Rangan, S. ; Katalinic, S. ; Thorpe, R. ; Bartynski, R. A. ; Rochford, J. ; Galoppini, E.: In: *J. Phys. Chem. C* 114 (2010), 1139 S.

[50] Hardman, P. J. ; Raikar, G. N. ; Muryn, C. A. ; Vanderlaan, G. ; Wincott, P. L. ; Thornton, G. ; Bullett, D. W. ; Dale, P.: In: *Phys. Rev. B* 49 (1994), 7170 S.

[51] Wang, Z. ; Helmersson, U. ; Käll, P.-O.: In: *Thin Solid Films* 405 (2002), 50 S.

[52] Liu, B. ; Wen, L. ; Zhao, X.: In: *Mater. Chem. Phys.* 106 (2007), 350 S.

[53] Cardona, M. ; Harbeke, G.: In: *Phys. Rev.* 137 (1965), A1467 S.

[54] Tiwald, T. E. ; Schubert, M.: In: *Proc. SPIE* 19 (2000), 4103 S.

[55] Hosaka, N. ; Sekiya, T. ; Satoko, C. ; Kurita, S.: In: *J. Phys. Soc. Jpn.* 66 (1997), 877 S.

[56] Aryasetiawan, F. ; Gunnarsson, O.: In: *Rep. Prog. Phys.* 61 (1998), 237 S.

[57] Görling, A.: In: *Phys. Rev. B* 53 (1996), 7024 S.

[58] Görling, A.: In: *Phys. Rev. A* 54 (1996), 3912 S.

[59] Görling, A. ; Levy, M.: In: *Phys. Rev. A* 50 (1994), 196 S.

[60] Grabo, T. ; Gross, E.K.U.: In: *Chem. Phys. Lett.* 240 (1995), 141 S.

[61] Jones, R. O. ; Gunnarsson, O.: In: *Rev. Mod. Phys.* 61 (1989), 689 S.

[62] Kümmel, S. ; Kronik, L.: In: *Rev. Mod. Phys.* 80 (2008)

[63] Kümmel, S. ; Perdew, J. P.: In: *Phys. Rev. B* 68 (2003), 035103 S.

[64] LABAT, F. ; BARANEK, P. ; DOMAIN, C. ; MINOT, C. ; ADAMO, C.: In: *J. Chem. Phys.* 126 (2007), 154703 S.

[65] SAGMEISTER, S.: *Excitonic Effects in Solids: Time-Dependent Density Functional Theory versus the Bethe-Salpeter Equation*, University Graz, Diss., 2009

[66] SHARMA, S. ; DEWHURST, J. K. ; AMBROSCH-DRAXL, C.: In: *Phys. Rev. Lett.* 95 (2005), 136402 S.

Acknowledgment

I want to thank my supervisor Claudia Ambrosch-Draxl for providing me with the opportunity to write this thesis and supporting me in scientific issues throughout. The nice working and social atmosphere she created in the group was very much appreciated.

I am most grateful to Andris Gulans who guided me through my first steps with the code and was always available to discuss various computational problems that arose. I am very thankful to Santiago Rigamonti and Stefan Kontur for discussions concerning excited states. I want to extend my thanks to Ute Werner for introducing me to the hybrid functionals in the code and Dmitrii Nabok for discussing G_0W_0 related issues. Furthermore, I am grateful to Pasquale Pavone and Matteo Guzzo for proofreading parts of the thesis.

Finally, I would like to thank my parents and Gregor for always encouraging and supporting me.

Selbständigkeitserklärung

Hiermit versichere ich, dass ich die vorliegende Arbeit selbständig verfasst und keine anderen als die angegebenen Quellen und Hilfsmittel verwendet habe.

Berlin, den

Unterschrift